International Journal of Earth Sciences
https://doi.org/10.1007/s00531-021-01995-0

ORIGINAL PAPER

From subduction to strike slip-related volcanism: insights from Sr, Nd, and Pb isotopes and geochronology of lavas from Sivas–Malatya region, Central Eastern Anatolia

Paolo Di Giuseppe[1] · Samuele Agostini[1] · Gianfranco Di Vincenzo[1] · Piero Manetti[2] · Mehmet Yilmaz Savaşçın[3] · Sandro Conticelli[2,4,5]

Received: 1 September 2020 / Accepted: 16 January 2021

Abstract

Anatolia is characterised by a complex geodynamic evolution, mirrored by a wide spectrum of magmatism. Here, we investigated the timing and the geochemical/isotopic characters of the Miocene to Pliocene volcanism of Sivas–Malatya Region (Central Eastern Anatolia), and its relationships with local and regional tectonics. Na-alkaline basaltic lavas were emplaced during middle Miocene at Sivas (16.7–13.1 Ma), in the North, whilst transition from calc-alkaline to Na-alkaline rocks is observed at Yamadağ and Kepez Dağ volcanic complexes. Calc-alkaline products erupted during early to middle Miocene, and more precisely from 19.5 to 13.6 Ma at Yamadağ and from 16.4 to 13.5 Ma at Kepez Dağ, with final Na-alkaline activity of the Arguvan volcanic field lasting till late Miocene (15.7–10.6 Ma). Volcanism renewed during the Pliocene in the Kangal (5.9–4.0 Ma) volcanic field with the emission of K-alkaline igneous rocks. Mafic calc-alkaline and Na-alkaline rocks partially overlap in age but can be easily distinguished by their petrochemical characters. Mafic calc-alkaline igneous rocks show typical subduction-related petrological and geochemical affinities. They are both two-pyroxene or clinopyroxene and amphibole-bearing rocks, characterised by high LILE/HFSE values, with variable $^{87}Sr/^{86}Sr_i$ (0.70396–0.70539) and $^{143}Nd/^{144}Nd_i$ (0.51260–0.51287). Mafic Na-alkaline igneous rocks are characterised by big olivine phenocrysts and show intraplate geochemical flavours, although some LILE depletion with respect to HFSE as well as variable $^{87}Sr/^{86}Sr_i$ (0.70347–0.70553) and $^{143}Nd/^{144}Nd_i$ (0.51261–0.51291) isotopic compositions are present. These characteristics are suggestive for the occurrence, at some stage of their genesis, of a possible interaction with subduction-related reservoirs. The Kangal K-alkali basalts still show intraplate-like petrological and geochemical affinities with LILE/HFSE ratios similar to those of the Miocene Na-alkaline rocks, and largely variable $^{87}Sr/^{86}Sr_i$ (0.70425–0.70520) and $^{143}Nd/^{144}Nd_i$ (0.51262–0.51277) isotopic compositions, overlapping the arrays observed in the earlier stages of volcanism. A general transition from calc-alkaline to Na-alkaline volcanic rocks is observed with time, according to the evolution of the geodynamics of the Anatolia region. Early to middle Miocene calc-alkaline magmas were derived by partial melting of the mantle wedge delimited by the subduction of the last oceanic branch of Neotethys. The Na-alkaline magmas, on the other hand, were generated within the asthenospheric mantle beneath the slab and migrated through slab tears into the mantle wedge where they mixed with subduction-related components. The subduction-related component decreased with time and transitional magmas are found in the youngest activity of Yamadağ and Kepez Dağ, shortly followed by clear within-plate lavas formed in the Arguvan volcanic field. The appearance of the youngest K-alkaline volcanic rocks in the Kangal basin represents an abrupt change in the magma supply at depth, although continental crustal contamination en-route to the surface played an important role in their genesis.

Keywords Sivas–Malatya · Isotope geochemistry · Miocene–Pliocene volcanism · Strike-Slip faulting

Introduction

The production of Na-alkaline magmas in post-collisional tectonic settings is related either to mantle upwelling and lithospheric thinning (e.g., Pearce et al. 1990) or to sub-lithospheric mantle flow through slab tears (e.g., Davies

✉ Samuele Agostini
s.agostini@igg.cnr.it

✉ Sandro Conticelli
sandro.conticelli@unifi.it; sandro.conticelli@cnr.it

Extended author information available on the last page of the article

Published online: 10 March 2021

and von Blanckenburg 1995). In this framework, intraplate magmas may be derived from either sub-continental lithospheric mantle (e.g., Hawkesworth and Gallagher 1993) or from asthenospheric mantle with possible contributions of earlier subduction-related reservoirs (e.g., White and McKenzie 1989).

In the Mediterranean and adjoining regions, post-collisional within-plate alkaline magmatism commonly occurs (e.g., Doglioni et al. 2002; Duggen et al. 2005; Lustrino and Wilson 2007; Cebriá et al. 2009; Conticelli et al. 2009; Seghedi et al. 2011; Dallai et al. 2019; Avanzinelli et al. 2020; Toscani et al. 2020).

In the Anatolia microplate, the intraplate alkaline post-collisional magmatism is widely found temporally and spatially distributed, although it can be clustered in three distinct periods of time:

(i) the first period, Miocene in age, occurred in the Thrace, Biga Peninsula, and Urla regions, in Western Anatolia (Yılmaz and Polat 1998; Aldanmaz 2002; Kaymakcı et al. 2007; Agostini et al. 2010a); in the Galatia and in Konya regions, in Central Anatolia (Keller et al. 1992; Wilson et al. 1997; Kurt et al. 2008; Gençoğlu Korkmaz et al. 2017); in the Sivas–Malatya and Mesudiye regions, in Central Eastern Anatolia (Kürkçüoğlu et al. 2015; Ekıcı 2016; Reid et al. 2019);

(ii) the second period, mainly Pliocene in age, followed in the Sivas–Malatya and Mesudiye regions, in Central Eastern Anatolia (Platzman et al. 1998; Ekıcı 2016; Koçaarslan and Ersoy 2018) and in the Karakoçan and Osmaniye regions, in Eastern Anatolia (Arger et al. 2000; Di Giuseppe et al. 2017);

(iii) the third period, Pleistocene in age, developed in the Kula region, in Western Anatolia (e.g., Innocenti et al. 2005), in the Cappadocia region, in Central Anatolia (Reid et al. 2017; Di Giuseppe et al. 2018; Dogan-Kulahci et al. 2018), in the Erzincan-Niksar, Osmaniye and Mesudiye regions, in North-Eastern Anatolia (Arger et al. 2000; Adıyaman et al. 2001; Tatar et al. 2007; Ekıcı 2016), and in the Elazığ region, in Eastern Anatolia (Arger et al. 2000; Di Giuseppe et al. 2017).

In the Anatolia microplate the volcanic activity is strictly associated with a long-term geodynamic history related with North–North-East subduction beneath the Eurasia Plate, forming, from west to east, the Hellenic and Cyprus arcs and the Bitlis Zagros Suture Zone, the latter as the consequence of the closure of Neo-Tethys and the middle Miocene collision of Arabia with Eurasia (e.g., Şengör and Yılmaz 1981; Dilek and Sandvol 2009). Neogene to recent volcanism in the Anatolia microplate mostly originated from mantle sources modified by a clear subduction signature (e.g., Innocenti et al. 1975; Pearce et al. 1990; Notsu et al. 1995; Alıci Şen et al. 2004, and reference therein). Post-collisional intraplate alkaline magmatism generally followed the subduction-related one although spatial and time overlaps are observed, and its products show a major contribution of ascending asthenospheric mantle (e.g., Adıyaman et al. 2001; Parlak et al. 2001; Di Giuseppe et al. 2017, 2018; McNab et al. 2018; Agostini et al. 2019). The shift from subduction-related to intraplate volcanism is poorly understood although relationships between the onset of Na-alkaline magmatism and local extension connected with a strike-slip tectonic regime are observed.

The Sivas–Malatya region is located between two of the most important strike-slip fault zones of Central Anatolia (Fig. 1), both belonging to the Central Anatolian Fault Zone, namely the sinistral NE–SW-trending Kızılırmak fault to the Westside and the sinistral N–S-trending Malatya-Ovacik fault in the East (e.g., Bozkurt 2001; Koçyigit et al. 2001). The magmatism of this region covers a wide time span, between early Miocene and middle Pliocene, with calc-alkaline and alkaline igneous rocks emplaced (e.g., Yılmaz et al. 1998; Platzman et al. 1998; Parlak et al. 2001; Kürüm et al. 2008; Ekıcı et al. 2009; Gürsoy et al. 2011; Kürkçüoğlu et al. 2015; Koçaarslan and Ersoy 2018; Reid et al. 2019), but a comprehensive and exhaustive geochronological and petrochemical study investigating also the shift from subduction-related to within-plate magmatism and its relationships with the local tectonic setting is still missing.

With this in mind, we report here new age (K–Ar and ^{40}Ar–^{39}Ar) determinations on seven selected samples to better constrain the time relationships among the five volcanic fields and complexes outcropping in the area. These data are matched and compared with a new detailed petrologic, geochemical, and isotopic (Sr–Nd–Pb) study on thirty-two representative samples of the magmatic rocks involved in the petro-chemical shift to post-collisional intraplate alkaline igneous rocks found in the Sivas–Malatya region. These are intimately related to but spatially separated with calc-alkaline ones. The new data are then discussed to: (i) reconstruct the time–space distribution of the magmatism of the region and its relationships with regional strike-slip faulting; (ii) identify the role of shallow level magmatic evolution (fractional crystallization and crustal contamination) in the differentiation of magmas; (iii) decipher the nature of the mantle sources involved in the magma genesis and their relationships with the tectonic evolution of the Anatolia microplate.

Samples studied and analytical methods, along with detailed petrographic data, are reported in full detail in the Electronic Supplementary Material (ESM 1).

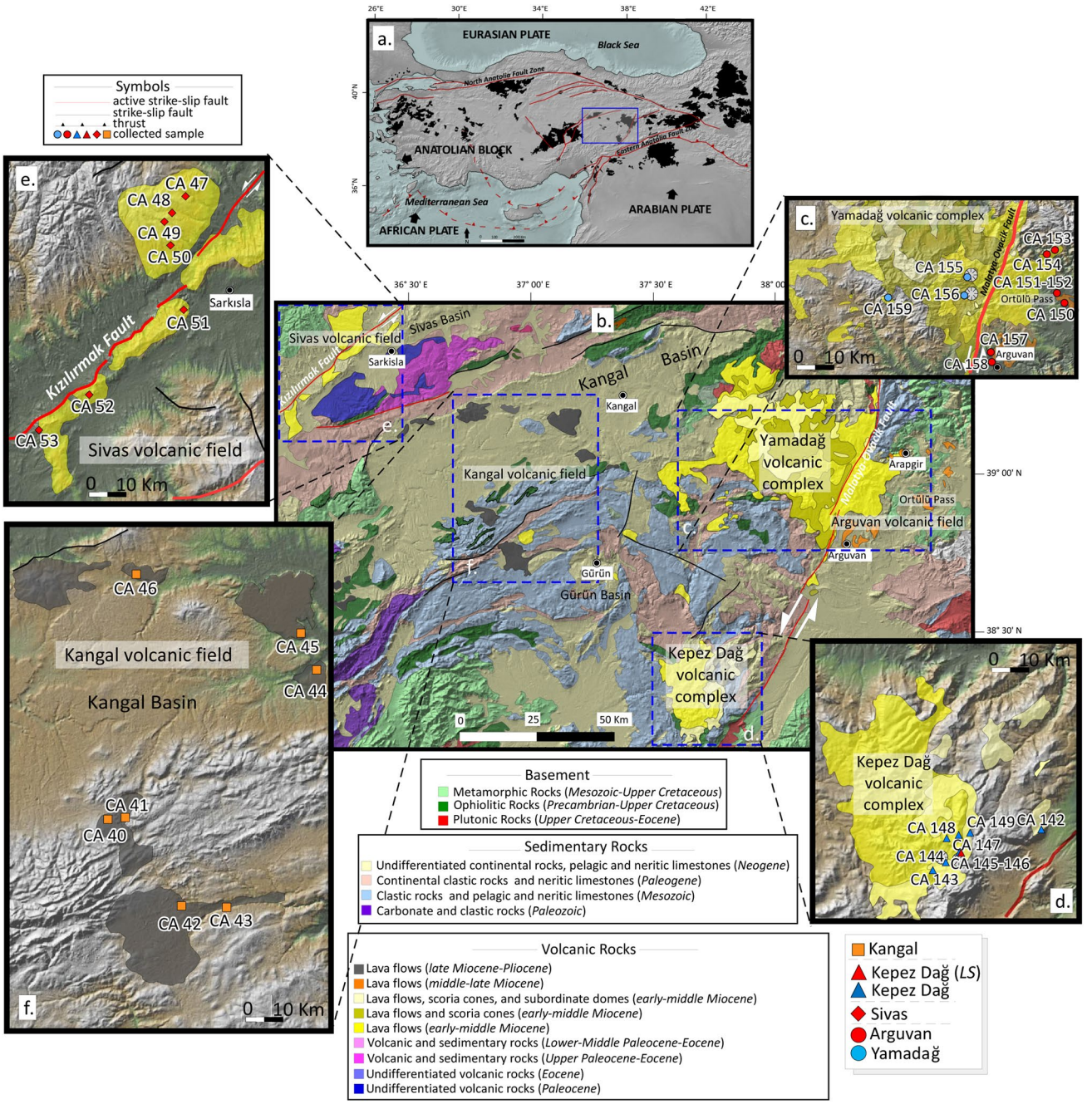

Fig. 1 **a** Sketch map of the Anatolia microplate showing the main tectonic features and the distribution of Neogene volcanism (in red). Big arrows represent the motion of the tectonic plates relative to Eurasia; dashed box indicates the study area enlarged in **b**; **b** simplified tectonic and volcanological map of the Central Eastern Anatolia Region. The region is subdivided into five different clusters here delimited by rectangles; **c** Yamadağ volcanic complex and Arguvan volcanic field; **d** Kepez Dağ volcanic complex; **e** Sivas volcanic field; **f** Kangal volcanic field

Geologic outline

The Anatolia microplate formed through the merging of several continental fragments during the complex geodynamic evolution of Paleao-Thetys and Neo-Tethys oceans (e.g., Şengör and Yılmaz 1981; Okay 2008; Dilek and Sandvol 2009). After the closure of the Neo-Tethys the collision of Africa-Arabia and Eurasia had a climax during middle Miocene, which brought to the formation of the Bitlis-Zagros Suture Zone (~ 13 Ma; Bozkurt 2001; Faccenna et al. 2006; Agard et al. 2011), at East, whilst the subduction of the African Plate beneath the Eurasian one

along the Cyprus and Aegean trenches continued in the West (e.g., Bozkurt 2001; Agostini et al. 2010b). During a collision, an initial tectonic regime of compressive deformation including thrusting, crustal shortening, thickening and plateau uplift (e.g. Anatolian-Iranian Plateau) was recorded in Central and Eastern Anatolia (e.g., Şengör and Yılmaz 1981; Şengör et al. 2003). During late Miocene, the tectonic regime switched from compressional to transcurrent, and this change is marked the onset of two main strike-slip faults, the E–W trending North Anatolia Fault (Şengör et al. 2005) and the SSW–NNE trending East Anatolian Fault (Bozkurt 2001; Fig. 1a). This new geodynamic and tectonic framework brought the formation, in the last 13 Ma, to the opening of several small pull-apart basins and an associated widespread tectonically-driven within-plate magmatism (e.g., Pearce et al. 1990; Şengör et al. 2003).

Volcanic outline and geochronology

The Sivas–Malatya region, located between Central and Eastern Anatolia, represents the north-eastern continuation of the of Cappadocia Volcanic Province (Fig. 1b). The volcanic region is delimited in the north-west by the Kızılırmak strike-slip fault and in the south-east by the Malatya-Ovacık strike-slip fault.

The volcanic activity is mainly concentrated along with these two main tectonic features, although a younger volcanic field occurs between the two fault zones, within the Kangal basin, which a SW–NE aligned intra-continental pull apart sedimentary basin (Boccaletti and Manetti 1988; Yağmurlu et al. 2016) (Fig. 1b).

Five different volcanic zones with rocks characterised by different petrographic features (Table 1) are recognised within the Sivas–Malatya region (Fig. 1). Although several geochronological data are available for this volcanism indicating a time span covering Miocene and Pliocene times (ESM 2), some uncertainty still persists with respect to the relationships among the different volcanic centres and between volcanism and tectonic features. To tackle this issue new K–Ar and ^{40}Ar–^{39}Ar data from the Sivas, Kangal, and Arguvan volcanic fields are reported in Table 2 and in Fig. 2 (full details of ^{40}Ar–^{39}Ar data in ESM 3). These data, along with geochronological data available in the literature, field relationships, and some petrographic details are herewith described.

The Yamadağ volcanic complex represents the oldest and largest volcanic centre of the region (Fig. 1b, c). It lies close to the Malatya-Ovacık fault zone, a 240 km long left-lateral strike-slip fault (e.g., Westaway and Arger 2001), which is considered as part of a more complex fault system related with the East Anatolia Fault (Westaway 2003). The volcanic succession of Yamadağ lays over the Tauride terranes, Carboniferous to Cretaceous in age (Yalçin et al. 1998), which mainly consist of sedimentary sequences and intermediate to silicic igneous rocks (e.g., lavas, pyroclastic products, domes, and dykes) ranging from kaolinitised rhyolitic breccia, ash-flow tuffs, and tuffisites, through basaltic andesitic and dacitic breccia, to trachy-andesite lavas (Yalçin et al. 1998). The volcanic activity of the Yamadağ volcanic complex was found to be within 19.5 and 13.6 Ma (Fig. 2a; ESM 2), and it is characterised by amphibole-bearing silicic to intermediate pyroclastic rocks and two-pyroxene andesitic to mafic lava flows (Table 1; ESM 1).

Younger ages, ranging from 10.1 to 9.7 Ma, were found for a basaltic lava sequence attributed to the Yamadağ volcanic complex (Gürsoy et al. 2011). The lack of any geochemical and petrological information on the dated samples cast doubts about their geological attribution, considering also that younger alkaline volcanic sequence of the Arguvan volcanic field lies unconformably on the older Yamadağ volcanic pile (see below).

The Arguvan volcanic field is made up by scattered olivine-bearing Na-alkaline basaltic lava flows (Table 1) overlying unconformably the calc-alkaline volcanic rocks of the Yamadağ volcanic complex (Fig. 1c) and rarely the rocks of the Tauride block. The volcanic activity of the Arguvan volcanic field developed through several monogenetic centres aligned along the Malatya-Ovacık strike-slip fault zone. Near the Arguvan village ouctrops a small sequence of four overlapping lava flows, other flows are found close to Arapgir village, and Ortülü Pass (Arger et al. 2000; Ekıcı et al. 2007) (Fig. 1c).

No age determinations of the volcanic rocks of Ortülü Pass area are available in the literature, and those of the Arguvan lava sequence were recently published by Reid et al. (2019) yielding an age of 10.9 Ma. On the other hand, previous K–Ar age determinations on olivine-bearing basaltic rocks from this volcanic field yielded ages between 15.9 and 15.2 Ma (Arger et al. 2000), which partially overlap the ^{40}Ar–^{39}Ar ages (i.e., 15.8–12.2 Ma) of rocks from the same area with some uncertainty on their stratigraphic position (Kürüm et al. 2008). We believe, however, that these ages are attributable to the Arguvan lavas on the basis of incompatible trace element ratios similar to those of intraplate-like rocks. Due to the uncertainties described above and to the relevance that Arguvan rocks have for the achievement of the main goals of the study, we performed two new ^{40}Ar–^{39}Ar determinations on samples well defined in terms of stratigraphic position, petrography and geochemistry (Table 1; Fig. 2a, b). The Ar–Ar data yielded an age of 15.60 ± 0.10 Ma ($\pm 2\sigma$) for a lava flow from Ortülü Pass area (CA 150) and age of 10.748 ± 0.066 Ma ($\pm 2\sigma$) for a lava flow near the Arguvan village (CA 158). These new data confirm that volcanism in the Arguvan volcanic field began almost coevally with that of

Table 1 Sample location, geology, petrography and mineralogy

Volcanic apparatus	Locality	Latitude (N)	Longitude (E)	Sample	Rock type	Series	Rock name	Texture	Paragenesis*
Kangal	Karakuyu	38° 52′ 52″	36° 48′ 09″	CA 40	Lava flow	K-Alkaline	K-Trachyandesite	Porphyritic + hypocrystalline gdm	**Ol** + **Plg** + **Opx** + plg + ol + cpx
Kangal	Karakuyu	35° 53′ 00″	36° 50′ 42″	CA 41	Lava flow	K-Alkaline	K-Trachyandesite	Porphyritic + hypocrystalline gdm	**Ol** + plg + ol + cpx
Kangal	Kaynarca	38° 45′ 39″	36° 58′ 58″	CA 42	Lava flow	K-Alkaline	K-Trachybasalt	Porphyritic + hypocrystalline gdm	**Ol** + **Cpx** + plg + ol + cpx
Kangal	Gürün	38° 45′ 14″	37° 08′ 41″	CA 43	Lava flow	K-Alkaline	Basalt	Porphyritic + hypocrystalline gdm	**Ol** + plg + ol + cpx
Kangal	Mancılık	39° 02′ 18″	37° 14′ 45″	CA 44	Lava flow	K-Alkaline	K-Trachyandesite	Porphyritic + hypocrystalline gdm	**Plg** + **Ol** + **Cpx** + **Opx** + plg + ol + cpx
Kangal	Beyyurdu	39° 06′ 48″	37° 10′ 17″	CA 45	Lava flow	K-Alkaline	Basalt	Porphyritic + hypocrystalline gdm	**Ol** + **Cpx** + plg + cpx + ol
Kangal	Altınyayla	39° 12′ 56″	36° 51′ 00″	CA 46	Lava flow	K-Alkaline	Basalt	Porphyritic + hypocrystalline gdm	**Ol** + **Cpx** + plg + ol + cpx
Kepez Dağ	Darıca-Elbistan	38° 18′ 51″	37° 39′ 10″	CA 145	Lava flow	Na-Alkaline	Basalt	Porphyritic + hypocrystalline gdm	**Plg** + **Ol** + **Cpx** + plg + cpx + ol
Kepez Dağ	Darende	38° 20′ 31″	37° 49′ 11″	CA 142	Lava flow	Calc-alkaline	Latite	Porphyritic + hypocrystalline gdm	**Plg** + **Ol** + **Cpx** + plg + cpx + ol + opx
Kepez Dağ	Darıca-Elbistan	38° 16′ 50''	37° 34′ 59″	CA 143	Lava flow	Calc-alkaline	Mugearite	Aphyric + hypocrystalline gdm	plg + ol
Kepez Dağ	Elbistan	38° 15′ 53″	37° 33′ 39″	CA 144	Lava dome	Calc-alkaline	Rhyolite	Porphyritic + vitrophyric gdm	**Plg** + **Hbl** + **Bt** + plg + hbl + bt
Kepez Dağ	Darıca	38° 18′ 51″	37° 39′ 10″	CA 146	Lava dome	Calc-alkaline	Dacite	Porphyritic + vitrophyric gdm	**Hbl** + **Plg** + plg + hbl
Kepez Dağ	Darıca	38° 20′ 41″	37° 38′ 39″	CA 147	Lava dome	Calc-alkaline	Benmoreite	Aphyric + hypocrystalline gdm	plg + ol + cpx + opx
Kepez Dağ	Darıca	38° 20′ 32″	37° 37′ 11″	CA 148	Lava flow	Calc-alkaline	Basaltic Andesite	Porphyritic + hypocrystalline gdm	**Ol** + plg + cpx + ol
Kepez Dağ	Darıca	38° 20′ 55″	37° 40′ 38″	CA 149	Lava dome	Calc-alkaline	Andesite	Aphyric + hypocrystalline gdm	plg + cpx
Sivas	Ortaköy	39° 28′ 38″	36° 16′ 49″	CA 47	Lava flow	Na-Alkaline	Basalt	Porphyritic + hypocrystalline gdm	**Ol** + plg + cpx + ol
Sivas	Ahrdal Koyüne	39° 28′ 04″	36° 15′ 32″	CA 48	Lava flow	Na-Alkaline	Basalt	Porphyritic + hypocrystalline gdm	**Ol** + **Cpx** + plg + ol + cpx
Sivas	Ortaköy	38° 27′ 18″	36° 15′ 35″	CA 49	Lava flow	Na-Alkaline	Basanite	Porphyritic + hypocrystalline gdm	**Ol** + **Cpx** + plg + ol + cpx
Sivas	Ortaköy	39° 50′ 52″	36° 15′ 27″	CA 50	Lava flow	Na-Alkaline	Basanite	Porphyritic + hypocrystalline gdm	**Ol** + plg + ol + cpx
Sivas	Ortatopaç	39° 22′ 32″	36° 16′ 29″	CA 51	Lava flow	Na-Alkaline	Basalt	Porphyritic + hypocrystalline gdm	**Ol** + **Cpx** + **Plg** + plg + cpx + ol
Sivas	Karagöl	39° 17′ 28″	36° 10′ 51″	CA 52	Lava flow	Na-Alkaline	Basalt	Porphyritic + hypocrystalline gdm	**Ol** + **Plg** + **Opx** + plg + ol + cpx
Sivas	Gemerek	39° 11′ 01″	36° 03′ 23″	CA 53	Lava flow	Na-Alkaline	Basalt	Porphyritic + hypocrystalline gdm	**Ol** + **Cpx** + **Plg** + plg + ol + cpx
Arguvan	Ortülü Pass	38° 53′ 10″	38° 35′ 13″	CA 150	Lava flow	Na-Alkaline	Basalt	Porphyritic + hypocrystalline gdm	**Plg** + **Cpx** + **Ol** + plg + cpx + ol
Arguvan	Ortülü Pass	38° 54′ 18″	38° 34′ 13″	CA 151	Lava flow	Na-Alkaline	Hawaiite	Porphyritic + hypocrystalline gdm	**Plg** + **Ol** + plg + ol + cpx
Arguvan	Ortülü Pass	38° 54′ 18″	38° 34′ 13″	CA 152	Lava flow	Na-Alkaline	Basalt	Porphyritic + hypocrystalline gdm	**Plg** + **Ol** + **Cpx** + plg + ol + cpx
Arguvan	Arapgir	39° 01′ 54″	38° 28′ 24″	CA 153	Lava flow	Na-Alkaline	Mugearite	Porphyritic + hypocrystalline gdm	**Plg** + **Ol** + plg + cpx + ol
Arguvan	Arapgir	39° 01′ 15″	38° 25′ 13″	CA 154	Lava flow	Na-Alkaline	Hawaiite	Porphyritic + hypocrystalline gdm	**Plg** + **Ol** + plg + ol + cpx

Table 1 (continued)

Volcanic apparatus	Locality	Latitude (N)	Longitude (E)	Sample	Rock type	Series	Rock name	Texture	Paragenesis*
Arguvan	Arguvan	38° 48′ 49″	38° 14′ 57″	CA 157	Lava flow	Na-Alkaline	Basalt	Porphyritic +hypocrystalline gdm	**Ol** + **Plg** + plg + ol + cpx
Arguvan	Arguvan	38° 47′ 41″	38° 15′ 41″	CA 158	Lava flow	Na-Alkaline	Basalt	Porphyritic +hypocrystalline gdm	**Ol** + plg + ol + cpx
Yamadağ	Yoncalı	38° 59′ 21″	38° 15′ 43″	CA 155	Lava dome	Calc-alkaline	Dacite	Porphyritic +vitrophyric gdm	**Plg** + **Hbl** + plg + hbl + opx
Yamadağ	Kömürlük	38° 53′ 32″	38° 14′ 38″	CA 156	Lava dome	Calc-alkaline	Basaltic Andesite	Porphyritic +hypocrystalline gdm	**Plg** + **Cpx** + plg + cpx
Yamadağ	Hekimhan	38° 50′ 25″	37° 50′ 02″	CA 159	Lava flow	Calc-alkaline	Andesite	Porphyritic +hypocrystalline gdm	**Plg** + **Hbl** + **Cpx** + plg + hbl

*Phenocrysts in bold

Table 2 K–Ar and ^{40}Ar–^{39}Ar age determinations of the selected samples

Sample	Group	Rock type	Dated fraction	Method	$^{40}Ar_{rad}$	$^{40}Ar_{rad}$ (%)	K–Ar age (Ma)
CA 42	Kangal	K-Trachybasalt	Groundmass	K–Ar	3.029×10^{-7}	59.9	4.79 ± 0.17
CA 44	Kangal	K-Trachyandesite	Groundmass	K–Ar	3.730×10^{-7}	75.8	5.11 ± 0.16
CA 48	Sivas	Basalt	Groundmass	K–Ar	2.825×10^{-7}	58.9	13.97 ± 0.47
CA 53	Sivas	Basalt	Groundmass	K-Ar	4.648×10^{-7}	35.0	15.71 ± 0.69
Sample	Group	Rock type	Dated fraction	Method	Weighted plateau age (Ma)	Total fusion age (Ma)	Isochron age (Ma)
CA 158	Arguvan	Basalt	Whole Rock	^{40}Ar–^{39}Ar	10.748 ± 0.066	10.79 ± 0.07	10.75 ± 0.07
CA 150	Arguvan	Basalt	Whole Rock	^{40}Ar–^{39}Ar	15.60 ± 0.10	15.58 ± 0.13	15.60 ± 0.10
CA 51	Sivas	Basalt	Whole Rock	^{40}Ar–^{39}Ar	15.737 ± 0.095	15.79 ± 0.10	15.75 ± 0.10

the Yamadağ volcanic complex, during the middle Miocene (Fig. 2a) protracting to the late Miocene (Fig. 2a).

The Kepez Dağ volcanic complex is located on the southwestern side of the Malatya-Ovacık strike-slip fault zone, just south of the Darende basin (Fig. 1d). It unconformably overlies the middle to upper Eocene Başören Formation of the Tauride block (e.g., Ekıcı et al. 2007). The volcanic activity of the Kepez Dağ volcanic complex gave ages within 16.4 and 14.1 Ma (Fig. 2a; ESM 2), and it is characterised by a volcanic sequence made up by amphibole-bearing silicic to intermediate pyroclastic rocks and two-pyroxene andesitic lava flows (Table 1; ESM 1). The Kepez Dağ rocks have, therefore, a clear calc-alkaline affinity on the basis of mineralogical and petrographic data (Table 1; ESM 1). However, Ekıcı (2016) recently reported the occurrence of scarce Na-alkali basalts at the top of the Kepez Dağ volcanic pile, with ages in the range of 14.0–13.6 Ma. These late-stage volcanic products (indicated as Kepez Dağ (LS) in Fig. 1d) represent the transition from subduction-related calc-alkaline to intraplate Na-alkaline feeded through the Malatya-Ovacık strike-slip fault, similarly to what is observed at the transition from the Yamadağ calc-alkaline volcanic rocks to the Arguvan Na-alkaline rocks.

The Sivas volcanic field is made up by scattered monogenetic lava flows and volcanic centres, lying along the Kızılırmak fault, at the southwest termination of the Sivas basin (Fig. 1e). The Sivas basin formed during the Triassic and it represents one of the largest intra-continental basins of Central Anatolia. The Kızılırmak fault separates the Anatolide–Tauride block, in the South, from the Kirşehir one, in the North (e.g. Yılmaz 1994; Dirik et al. 1999; Fig. 1e). The Sivas volcanic field straddles the Kızılırmak fault with volcanic rocks belonging to the Na-alkaline suite (e.g., Platzman et al. 1998; Parlak et al. 2001; Kürkçüoğlu et al. 2015). The lava flows of the Sivas volcanic field are olivine-bearing, single-pyroxene (clino-) basalts, with big euhedral olivine phenocrysts, indicating that they belong to an alkaline suite (Table 1; ESM 1). Geochronological data from the literature (ESM 2) give ages ranging from 16.7 to 13.1 Ma (e.g., Platzman et al. 1998; Reid et al. 2019). This time span is well within the range of calc-alkaline volcanic activity of Yamadağ and Kepez Dağ volcanic complexes. To confirm the chronological succession of volcanic and tectonic events, we selected three samples from Sivas volcanic field for new K–Ar and ^{40}Ar–^{39}Ar determinations (Table 2). The samples collected close to the Kızılırmak fault (Fig. 1e) yielded K–Ar ages of 14.0 ± 0.5 Ma and 15.7 ± 0.7 Ma (CA 48 and

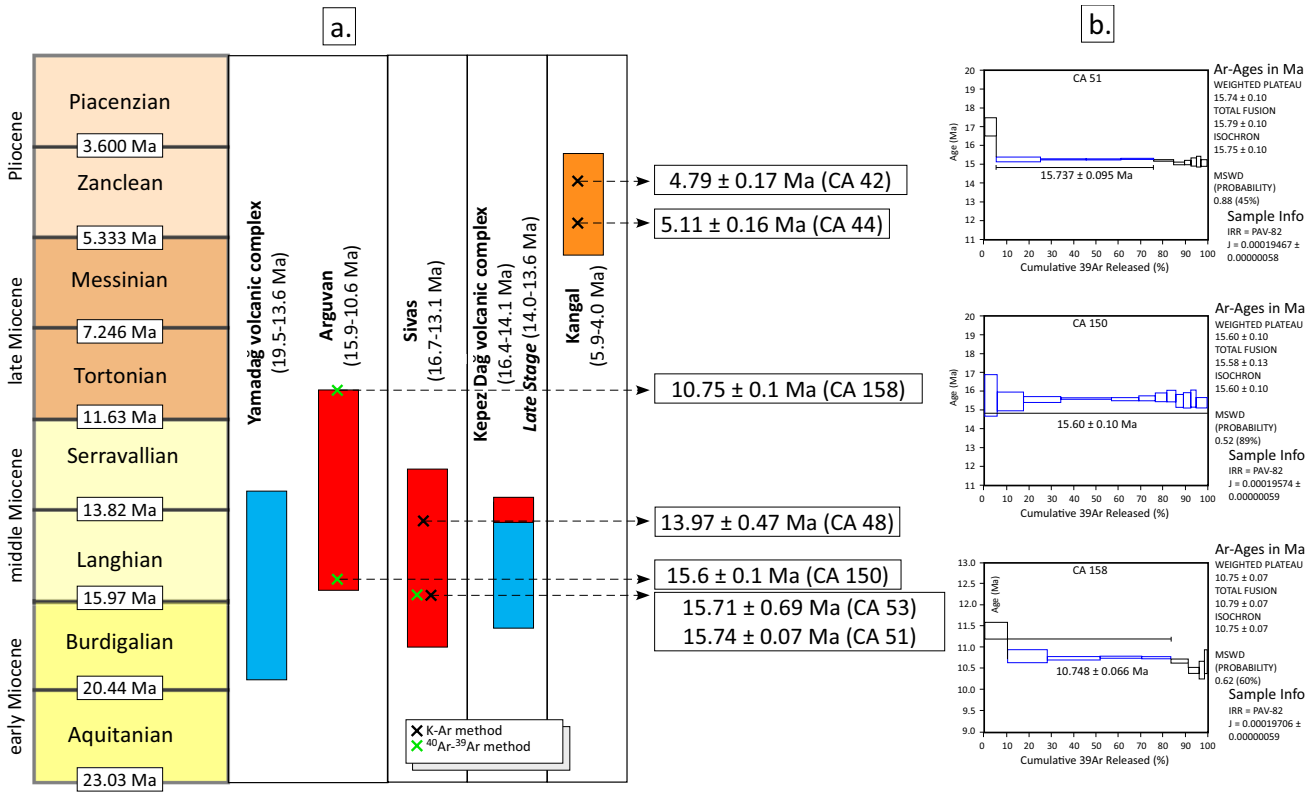

Fig. 2 **a** Simplified chronostratigraphic map showing the volcanic activity of the study area (data in ESM 2). New K–Ar and ^{40}Ar–^{39}Ar age determinations are also reported; **b** ^{40}Ar–^{39}Ar age spectra of analysed samples

CA 53, respectively), whereas the groundmass of sample CA 51 yelded a ^{40}Ar–^{39}Ar age of 15.737 ± 0.095 Ma (Table 2). These results narrow the previous time span recorded (16.8–13.1 Ma, Platzman et al. 1998; Reid et al. 2019), but confirm that the intraplate Na-alkaline magmatic rocks along the Kızılırmak fault are slightly older than the outpouring of intraplate Na-alkaline magmas along the Malatya-Ovacık strike-slip fault.

The Kangal volcanic field is made up by small and scattered lava plateaus and monogenetic volcanic centres lying within the Kangal basin (Fig. 1f). The Kangal basin is a SW–NE oriented sedimentary basin running parallel to the Sivas basin and delimited by the Kızılırmak and Malatya-Ovacık strike-slip faults. The substratum of the Kangal volcanic field is made up by metamorphic terranes belonging the Anatolide–Tauride block (e.g., Poisson et al. 2016; Yağmurlu et al. 2016). The Kangal volcanic rocks are prevalently olivine-bearing, single-(clino-)pyroxene basalts (Table 1; ESM 1), where fresh olivine, often iddingsite-rimmed, has euhedral to skeletal textures indicating its rapid growth in alkaline magmas (Conticelli 1998). Geochronological data available for Kangal volcanic rocks yielded ages in the range between 5.9 and 4.0 Ma (ESM 2), which differs from the isotopic ages found for similar lavas in the adjacent Gürün basin, immediately South of the Kangal basin, that yielded ages in the range between 19.9 and 17.5 (Reid et al. 2019). To tackle these discrepancies two samples (CA 42, CA 44) from Kangal were analysed for age determination. The analyses yielded K–Ar ages of 4.8 ± 0.2 and 5.1 ± 0.2 Ma, respectively (Table 2; Fig. 2a, b). These new data are well within the values found in the recent literature (see ESM 2) confirming that volcanic activity within the basis is much younger than along Kızılırmak and Malatya-Ovacık strike-slip faults.

Classification

The complete set of major element chemistry of the samples used in this study are reported in the ESM 4. Figure 3a shows the plot of $Na_2O + K_2O$ *vs.* SiO_2 on a water-free basis (i.e., Total Alkali-Silica diagram—TAS; Le Maitre 2002) for the entire set of analysed samples along with the alkaline-subalkaline divide proposed by Irvine and Baragar (1971).

Volcanic rocks from Kepez Dağ and Yamadağ volcanic complexes are clearly sub-alkaline, and they fall below the divide (Fig. 3a), according to their petrographic characteristics. They range in composition from olivine-bearing basaltic andesite to rhyolite (Fig. 3a). Using the K_2O vs. SiO_2 diagram (Fig. 3b; Ewart 1982) the Kepez Dağ and Yamadağ

volcanic rocks straddle partially the calc-alkaline and high-K calc-alkaline fields. On the other side, Arguvan and Sivas volcanic rocks straddle the alkaline/sub-alkaline divide, whilst only the youngest lavas of Kangal volcanic field are clearly alkaline plotting above the divide (Fig. 3a). The Total Alkali-Silica diagram, however, does not distinguish between sodic and potassic alkaline suites. Therefore, to better constrain the classification of these alkaline suites, the K_2O vs. Na_2O diagram is further used (Middlemost 1975), which indicates that Sivas and Arguvan volcanic rocks are Na-alkaline whereas those from Kangal basin are alkaline-potassic (Fig. 3c). Therefore, the Arguvan volcanic rocks range in composition from basanites to tephrites and alkali olivine basalts, whereas Sivas rocks range from hawaiites to alkali olivine basalts. The Na-alkaline serial affinity agrees with the mineralogical features of Sivas and Arguvan volcanic rocks where olivine has euhedral textures and orthopyroxene is constantly missing (ESM 1).

Kangal volcanic rocks have a clear alkaline potassic nature (Fig. 3c) with samples ranging in composition from potassic alkali basalts to potassic trachybasalts, and potassic trachyandesites. We would like to remark that the term shoshonite is widely used for alkaline-potassic trachyandesite when found in subduction-related settings. In this case, we prefer to maintain the generic term potassic trachyandesite rather than the specific one because of their possible within-plate genesis.

In summary, calc-alkaline rocks are restricted to the early-middle Miocene volcanic complexes aligned along the Malatya-Ovacık strike-slip fault, whilst Na-alkaline volcanic rocks are found at the end of the calc-alkaline igneous activity, from the middle to late Miocene and coevally along the Kızılırmak strike-slip fault. Potassic-alkaline rocks are Pliocene in age and found within the basin delimited by the Kızılırmak and Malatya-Ovacık strike-slip faults.

Chemical and isotopic data

Whole-rock geochemistry

Major and trace element compositions of selected samples are reported in Table 3 and in ESM 4. CIPW norms are also reported in ESM 4. The Kepez Dağ and Yamadağ volcanic rocks show the largest compositional range among the five different volcanic systems of the Sivas–Malatya region (Fig. 3a), with SiO_2 and MgO ranging from 48.2 to 68.7 wt% and from 1.05 to 8.50 wt%, respectively. The igneous rocks from Arguvan volcanic field are mostly mafic in composition with a narrow range of silica (49.2–49.6 wt%) but largely variable in magnesia (MgO = 5.63–9.15 wt%) and alkali ($Na_2O + K_2O$ = 3.31–5.61 wt%) contents (ESM 4). The igneous rocks from the Sivas volcanic field are also mostly mafic but with a larger range of silica (43.0–50.2 wt%) and MgO (8.33–14.1 wt%; ESM 4) contents than Arguvan rocks. It should be pointed out that some Na-alkaline rocks are actually *olivine-hypersthene* normative and fall under the alkaline-subalkaline divide (Fig. 3a). The Kangal volcanic rocks show larger compositional range than other alkaline rocks of the region. They have silica and magnesia contents ranging from 47.3 to 52.1 wt% and from 5.48 to 9.10 wt% (ESM 4), respectively, with MgO significantly higher than those of the calc-alkaline rocks at a given SiO_2. Differently from the Sivas and Arguvan basalts, the Kangal volcanic rocks are potassium-rich (Fig. 3c).

The narrow range in silica contents observed in the alkaline rocks from Sivas, Arguvan, and Kangal volcanic areas limit its efficiency to describe the differentiation of each volcanic suite. MgO was then selected as differentiation index and thus several lines of descent are defined even though in the cases of monogenetic volcanic activity the compositional ranges are extremely restricted. Variation diagrams of MgO vs. selected elements are reported in Fig. 4; a more comprehensive set of variation diagrams vs. major and trace elements is shown in ESM Fig. 5a–d). Calc-alkaline rocks from Yamadağ and Kepez Dağ volcanic complexes commonly exhibit well-defined positive trends for TiO_2, Fe_2O_3, MnO, CaO and P_2O_5, negative for SiO_2 and Na_2O and scattered for K_2O and Al_2O_3. They are also characterised by the positive correlation of MgO with respect to all of the Transition Elements (e.g., V, Cr, Co and Ni). Large Ion Lithophile Elements (LILE), in contrast, show negative trends for Rb and Ba, and weakly positive for Sr, whereas High Field Strenght Elements (HFSE) display slightly positive trend for Nb and the absence of any trend for Zr.

Na-alkaline rocks from Sivas and Arguvan volcanic fields show positive trends for CaO, Fe_2O_3, MnO, Cr, Co, and Ni and negative trends for Al_2O_3, SiO_2, Na_2O, K_2O, and V with increasing MgO. Negative trends with increasing MgO are also observed for Rb, Ba, and Sr although in some cases the restricted range of MgO of the Arguvan lavas does not permit to clearly define the correlation for these rocks (Fig. 4; ESM Fig. 5). HFS elements display complex correlations.

Potassic alkaline rocks from Kangal volcanic field show trace element trends similar to those observed for the Na-alkaline rocks. HFS elements, and especially Nb and Ta have concentration levels consistently higher than those observed in all of the other rocks studied at the same level of MgO (Fig. 4; ESM Fig. 5).

Rare Earth Element (REE) chondrite-normalised distributions show fractionated patterns for light and medium REE and relatively low high REE contents, with the exception of late Miocene Arguvan volcanic rocks showing flat trend of heavy REE (ESM Fig. 5e). Multi-element diagrams normalised to the primordial mantle show significant differences in the patterns of the calc-alkaline rocks with respect to those

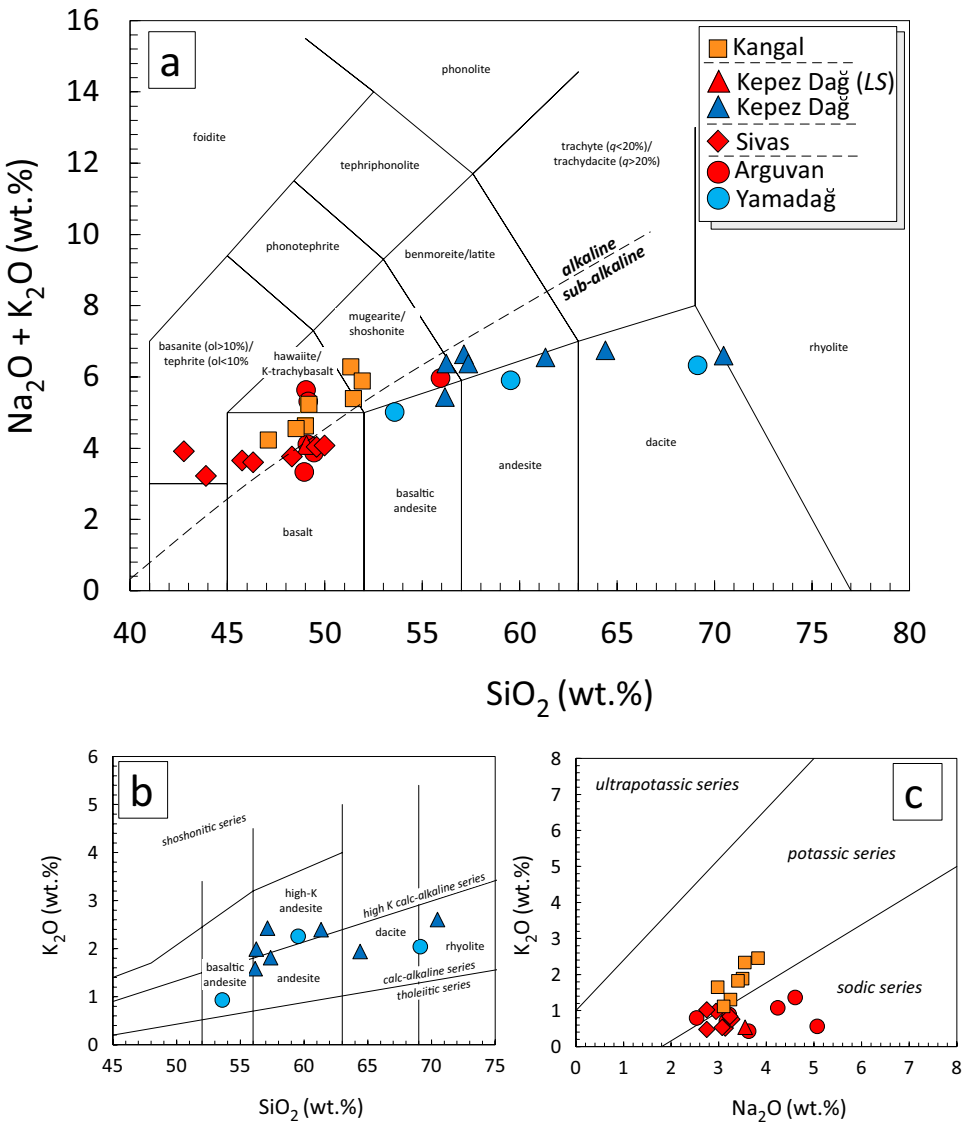

Fig. 3 Classification diagrams for the studied rocks: **a** TAS classification diagram (Le Maitre 2002). Dashed line indicates the boundary between alkaline and sub-alkaline fields according to Irvine and Baragar (1971); **b** K_2O vs. SiO_2 diagram (Ewart 1982); **c** K_2O vs. Na_2O diagram (Middlemost 1975)

of the Na- and K-alkaline (Fig. 5). Calc-alkaline rocks of Yamadağ and Kepez Dağ volcanic complexes show patterns typical of subduction-related igneous rocks (Hofmann 1997), with Ba, U and Pb peaks and Ta, Nb, and Ti troughs (Fig. 5a, b). The Na-alkaline and K-alkaline igneous rocks of Sivas, Arguvan and Kangal volcanic fields show different patterns (Fig. 5a, c, d), which mainly resemble those of intra-plate volcanic rocks but with some discrepancies with respect to typical Ocean Island Basalts and OIB-like within-plate volcanic rocks (Hofmann 1997). Indeed, the Na-alkaline rocks from Sivas show bell-shaped patterns, still showing weak negative anomalies in Nb, Ta, and Ti (Fig. 5c). On the other hand, the Na-alkaline Arguvan lavas display patterns less enriched in incompatible elements with respect to OIB, although with smaller negative anomalies in Nb and Ta, with respect to the Sivas Na-alkaline rocks, and no anomaly in Ti (Fig. 5a). The basalt belonging to the Late Stage activity of Kepez Dağ show low degree of enrichments in the most incompatible elements (e.g. Cs, Rb, Ba, Th and U) as well as smaller negative Nb–Ta and positive Pb spikes with respect to calc-alkaline samples, and almost flat REEs (Fig. 5b and Fig. ESM 5e). The K-alkaline volcanic rocks from Kangal volcanic field are the most enriched in incompatible elements and display linear patterns comparable to OIB but with no negative anomalies in K and Pb (Fig. 5e).

In summary, early to middle Miocene calc-alkaline and early-late Miocene to Pliocene alkaline rocks are characterised by different patterns in multi-element variation diagrams indicating a derivation from different magmatic sources, although some transitional features are observed.

Table 3 Major elements and trace elements of selected samples

Sample	CA 156	CA 150	CA 153	CA 154	CA 158	CA 48	CA 50	CA 53	CA 146	CA 148	CA 145	CA 41	CA 43	CA 44
Apparatus	YD	A	A	A	A	Si	Si	Si	KD	KD	KD (LS)	KA	KA	KA
Rock type	Basaltic Andesite	Basalt	Mugearite	Hawaiite	Basalt	Basalt	Basanite	Basalt	Dacite	Basaltic Andesite	Basalt	K-Trachyandesite	Basalt	K-Trachyandesite
SiO_2 (wt%)	53.1	48.5	55.7	48.7	47.6	45.9	43.3	49.8	63.7	55.3	48.2	51.0	48.9	51.8
TiO_2	1.40	1.49	1.53	2.26	1.70	1.29	1.47	1.68	0.80	1.11	1.40	2.16	2.24	2.05
Al_2O_3	17.1	16.3	18.3	18.2	14.9	14.6	12.6	14.5	17.3	16.1	16.7	15.6	15.2	16.2
Fe_2O_3	1.38	2.84	4.01	2.21	2.99	2.41	3.11	3.48	0.81	3.09	2.00	2.43	1.76	4.06
FeO	6.95	7.39	3.85	7.99	7.47	9.74	8.33	7.75	2.92	3.66	7.62	7.52	8.75	5.81
MnO	0.13	0.15	0.12	0.14	0.14	0.16	0.16	0.15	0.06	0.10	0.15	0.14	0.15	0.13
MgO	4.58	8.19	2.62	5.61	8.42	9.63	13.9	8.83	1.75	5.73	8.50	5.67	7.93	5.49
CaO	8.43	8.58	6.74	7.41	8.65	10.3	11.2	8.28	4.44	7.43	8.66	7.15	8.78	7.35
Na_2O	4.05	3.57	4.58	4.20	3.12	3.04	2.71	3.22	4.76	3.80	3.49	3.80	2.97	3.54
K_2O	0.92	0.42	1.36	1.07	0.87	0.53	0.47	0.84	1.92	1.56	0.53	2.44	1.64	2.33
P_2O_5	0.25	0.16	0.30	0.45	0.24	0.33	0.50	0.24	0.17	0.23	0.18	0.59	0.45	0.43
LOI	1.07	1.95	0.96	1.11	3.09	0.76	2.33	1.69	0.32	1.01	2.96	0.93	1.32	0.87
Total	99.36	99.56	100.07	99.36	99.21	98.74	100.04	100.53	98.94	99.14	100.35	99.45	100.05	100.04
Mg#	55.87	63.40	45.18	55.98	63.53	62.98	72.45	63.06	53.73	66.81	65.49	57.78	61.73	57.62
Trace elements (μg/g)														
Sc	–	31	–	17	–	22	20	22	8	22	27	18	21	27
V	203	201	197	158	204	172	175	173	72	145	171	192	211	233
Cr	60	200	20	16	320	248	535	253	4	189	250	164	263	226
Co	29	47	24	37	46	58	63	48	13	26	40	36	44	35
Ni	30	98	< 20	46	140	224	432	229	9	93	120	77	135	83
Cu	50	55	40	29	50	61	75	69	23	24	40	26	48	28
Ga	21	18	23	19	22	19	16	21	23	17	16	24	22	21
Rb	21	12	32	14	9	8	4	9	69	50	23	55	27	47
Sr	365	258	453	635	1100	467	724	344	356	414	426	572	544	509
Y	27	28	29	32	19	22	21	20	17	20	22	29	24	26
Zr	149	120	178	235	116	83	116	110	198	164	113	243	185	215
Nb	12	5	12	20	13	11	22	11	11	10	5	37	28	30
Cs	0.4	8.2	0.7	0.2	0.2	0.3	0.7	0.3	3.2	2.5	1.5	0.5	0.7	0.3
Ba	151	69	233	190	111	288	360	106	299	272	69	413	393	411
La	21.8	7.90	22.5	21.5	12.8	22.2	37.4	12.1	19.0	20.0	8.2	38.2	25.4	29.6
Ce	38.3	19.4	43.4	45.5	26.9	46.4	76.3	25.7	41.1	39.2	19.0	76.7	53.2	63.0
Pr	4.61	2.80	5.05	5.90	3.27	5.73	8.84	3.34	4.80	4.40	2.59	9.29	6.58	7.30
Nd	18.9	12.6	20.4	24.9	14.5	22.2	33.6	14.1	18.3	17.9	12.4	36.8	27.0	29.7
Sm	4.4	3.3	4.6	4.7	3.6	4.4	6.0	3.8	3.4	3.3	3.4	7.7	6.0	6.4

Table 3 (continued)

Sample	CA 156	CA 150	CA 153	CA 154	CA 158	CA 48	CA 50	CA 53	CA 146	CA 148	CA 145	CA 41	CA 43	CA 44
Eu	1.57	1.10	1.58	1.60	1.37	1.32	1.71	1.37	1.00	1.00	1.14	2.12	1.82	1.92
Gd	4.8	4.0	5.0	5.4	4.0	4.3	5.2	4.0	3.6	3.2	3.5	6.5	5.4	6.0
Tb	0.80	0.70	0.82	0.90	0.62	0.67	0.75	0.65	0.50	0.60	0.60	1.00	0.83	0.92
Dy	4.9	5.3	4.9	5.9	3.7	3.8	3.9	3.7	3.3	3.2	4.0	5.2	4.5	5.2
Ho	0.97	1.00	0.96	1.10	0.71	0.81	0.76	0.72	0.60	0.60	0.80	1.00	0.86	1.00
Er	2.8	3.0	2.9	3.0	1.9	2.1	1.9	1.9	1.6	1.9	2.4	2.5	2.2	2.7
Tm	0.41	0.40	0.41	0.40	0.24	0.29	0.25	0.24	0.20	0.20	0.34	0.32	0.27	0.36
Yb	2.7	2.8	2.7	2.7	1.5	1.7	1.5	1.5	1.6	1.7	2.3	2.0	1.7	2.2
Lu	0.41	0.40	0.42	0.40	0.22	0.24	0.21	0.21	0.30	0.30	0.36	0.27	0.24	0.32
Hf	3.3	2.7	3.8	4.9	2.6	2.0	2.6	2.8	4.7	3.6	2.3	5.7	4.4	5.3
Ta	0.7	0.3	0.7	1.1	0.7	0.6	1.2	0.7	0.7	0.6	0.2	2.5	1.9	1.9
Pb	5.0	1.6	9.0	3.2	5.0	2.9	5.0	4.6	13.7	11.3	5.0	8.3	5.8	8.1
Th	3.6	1.2	4.6	2.5	1.4	3.9	6.7	1.8	7.0	7.9	1.4	6.5	3.9	6.6
U	1.1	0.3	1.4	0.8	0.4	0.9	1.5	0.6	2.2	2.3	0.5	1.3	1.1	1.6

YD Yamadağ volcanic complex, *KD* Kepez Dağ volcanic complex, *Si* Sivas volcanic field, *A* Arguvan volcanic field, *Kangal* volcanic field, $Mg\text{-}\# = 100 \times ([MgO]/([MgO] + 0.85 \times [FeOtot]))$; figures of data agree with precision of measurements

Sr, Nd and Pb isotopes

Sr, Nd and Pb isotopes were measured on 14 representative samples; initial isotopic values were corrected on the basis of available K–Ar and ^{40}Ar–^{39}Ar age data (Table 4). Calc-alkaline rocks from Yamadağ and Kepez Dağ volcanic complexes show $^{87}Sr/^{86}Sr_{(i)}$ and $^{143}Nd/^{144}Nd_{(i)}$ within the ranges 0.70396–0.70539 and 0.51260–0.51287, respectively. These values are similar to those of Quaternary calc-alkaline volcanic rocks from Cappadocia Volcanic Province (Reid et al. 2017; Dogan-Kulahci et al. 2018; Di Giuseppe et al. 2018). Coeval Na-alkaline rocks from Sivas volcanic field also display a large range of $^{87}Sr/^{86}Sr_{(i)}$ and $^{143}Nd/^{144}Nd_{(i)}$ varying from 0.70414 to 0.70553 and from 0.51261 to 0.51282. Late Miocene Na-alkaline volcanic rocks from Arguvan volcanic field, on the other hand, display a narrower range than the other groups previously reported, with $^{87}Sr/^{86}Sr_{(i)}$ and $^{143}Nd/^{144}Nd_{(i)}$ ranging from 0.70347 to 0.70432 and from 0.51277 to 0.51291, which are the closest values to the mantle end members (Fig. 6). The late-stage Kepez Dağ basalts (CA 145) has intermediate values between older Kepez Dağ samples and Arguvan basalts (i.e.$^{87}Sr/^{86}Sr_{(i)}$ and $^{143}Nd/^{144}Nd_{(i)} = 0.70465$ and 0.51274, respectively). K-alkaline volcanic rocks from Kangal volcanic field show, similarly to the Sivas Na-alkaline rocks, the largest range in $^{87}Sr/^{86}Sr_{(i)}$ and $^{143}Nd/^{144}Nd_{(i)}$, from 0.70425 to 0.70520 and from 0.51262 to 0.51277, respectively. These values overlap the narrow field of Miocene to Quaternary volcanic rocks of Anatolia microplate (Fig. 6), belonging to the Elazığ Volcanic Province (Di Giuseppe et al. 2017), to the Kızılırmak and Acıgöl-Nevşehir volcanic areas of the Cappadocia Volcanic Province (Di Giuseppe et al. 2018), and the Kula area (Innocenti et al. 2005).

The Miocene–Pliocene igneous rocks of the Sivas–Malatya region show a large spectrum of lead isotopic compositions overlapping the entire range observed for the Anatolia volcanic rocks (Fig. 7a, b). The lowest values of $^{206}Pb/^{204}Pb_{(i)}$ (18.522–18.683) and $^{208}Pb/^{204}Pb_{(i)}$ (38.581–38.804) and among the lowest values of $^{207}Pb/^{204}Pb_{(i)}$ (15.635–15.650) are shown by the K-alkaline rocks of Kangal, which are the youngest ones of the region (Fig. 7). These values fall partially outside of the known range of Miocene to Quaternary Anatolian volcanic rocks. On the other hand, the highest values of $^{206}Pb/^{204}Pb_{(i)}$ (18.953–19.105) and $^{208}Pb/^{204}Pb_{(i)}$ (39.013–39.238) and among the highest values of $^{207}Pb/^{204}Pb_{(i)}$ (15.681–15.707) are shown by the Na-alkaline rocks of Sivas volcanic field (Fig. 7). Calc-alkaline volcanic rocks of Yamadağ and Kepez Dağ and Na-alkaline rocks from Arguvan display intermediate values (Fig. 7). Overall, the samples studied to define a fairly positive array running parallel, but well above, to the Northern Hemisphere Reference Line (NHRL; Hart 1984).

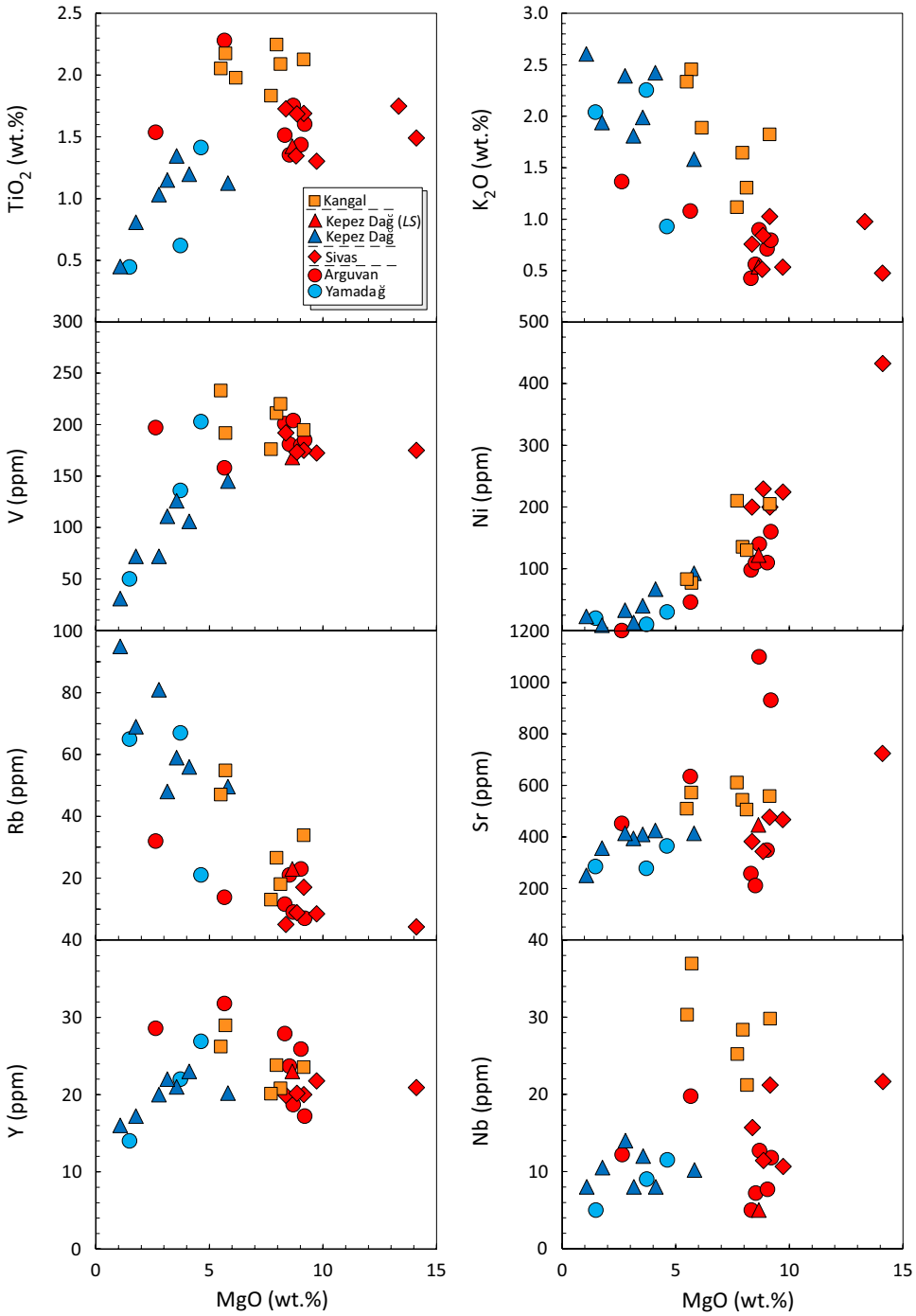

Fig. 4 Selected major and trace element vs. MgO (recalculated on a LOI-free basis) diagrams

Discussion

The field and geochronological data corroborate the fact that Miocene magmatism is strictly related to the Malatya-Ovacık and the Kızılırmak strike-slip faults. Indeed, the Yamadağ and Kepez Dağ volcanic complexes are aligned along the Malatya-Ovacık strike-slip fault, whereas the monogenetic volcanic centres of Sivas volcanic field are aligned along the Kızılırmak strike-slip fault. In addition, also the transition from calc-alkaline to Na-alkaline volcanism appears to be related to the main tectonic features of the area. Na-alkaline volcanic rocks are, indeed, erupted later than calc-alkaline rocks (Fig. 2), whilst the potassic alkaline rocks are the youngest and erupted far from the two main tectonic lineaments of the area, well within the Kangal basin (Fig. 1b).

The two large calc-alkaline volcanic complexes in the area (i.e., Yamadağ and Kepez Dağ) are aligned on the

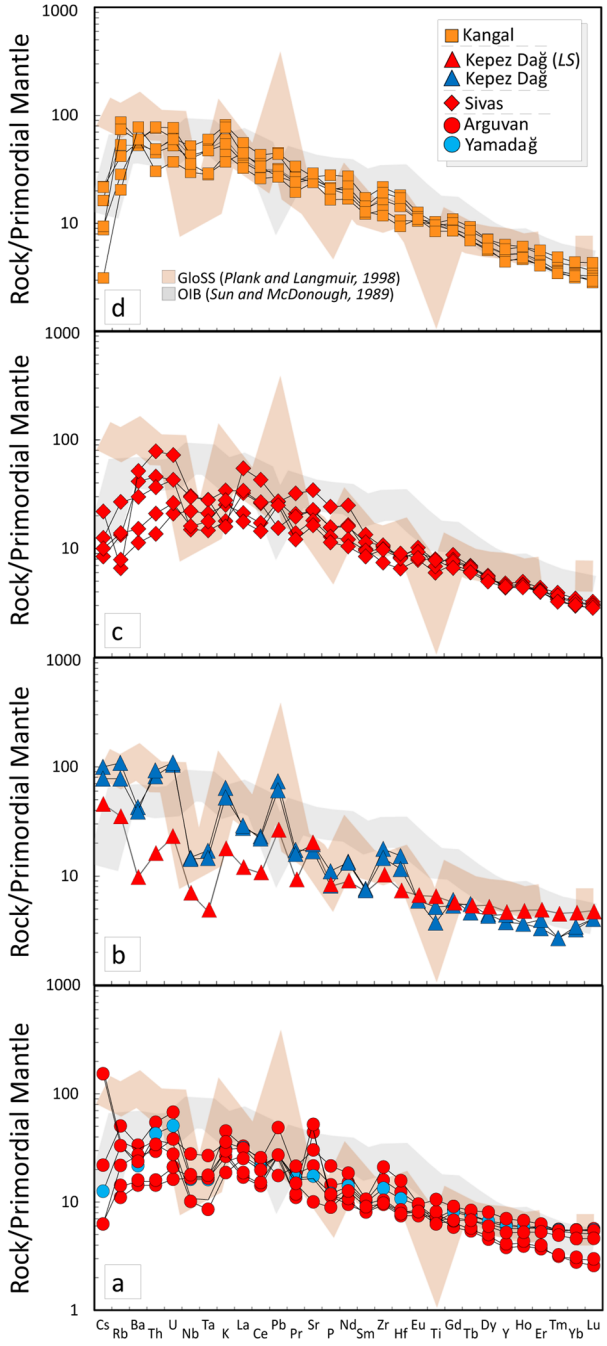

Fig. 5 Primitive mantle (PM)-normalised diagrams for the studied calc-alkaline rocks from Yamadağ and Kepez Dağ (**a**, **b**), Na-alkaline rocks from Arguvan and Sivas and (**a**–**c**), and K-alkaline rocks from Kangal (**d**). Light grey area represents the typical OIB composition, whereas light brown trend represents the average GloSS (Global Subduction Sediments) composition. Primitive mantle and OIB values are from Sun and McDonough (1989); GloSS composition is from Plank and Langumir (1998)

Malatya-Ovacık strike-slip fault and both volcanoes show late-stage emplacement of lava flows, which are either transitional to Na-alkaline, at Kepez Dağ, or clearly Na-alkaline, at Yamadağ with the emplacement of the Arguvan lavas (Figs. 1b and 2).

To the North-West, along the Kızılırmak strike-slip fault, the Sivas volcanic rocks developed coevally with the calc-alkaline ones of the Yamadağ and Kepez Dağ volcanic complexes (Figs. 1b and 2). It is characterised by Na-alkaline products, with some transitional geochemical features (Figs. 3 and 5).

The late Miocene to Pliocene volcanic activity of the Kangal volcanic field, which is found in the centre of the homonymous sedimentary basin delimited to the North and to the South by regional strike-slip faults (Figs. 1b and 2), further complicates the scenario of this area. Differently from other surrounding volcanic succession (i.e., Cappadocia at West or Elaziğ at East), the Kangal alkaline lavas exhibit an uncommon enrichment of K rather than Na (Fig. 3) with a clear within-plate signature (Fig. 5). This puts further complexity to the tectono-magmatic evolution of Central Eastern Anatolia (Di Giuseppe et al. 2017).

In summary, the following questions arise from the study of the Sivas–Malatya region: (i) what are the relationships between the coeval calc-alkaline and Na-alkaline volcanisms found along the Kızılırmak and the Malatya-Ovacık strike-slip faults?; (ii) is there any relationship between the subduction-related calc-alkaline volcanic activity of the Yamadağ and Kepez Dağ volcanic complexes and the Kızılırmak strike-slip fault?; (iii) what is the relationship between the Yamadağ calc-alkaline volcanic activity and the overlying Arguvan Na-alkaline lava flows?; (iv) as a corollary, are the Kızılırmak and the Malatya-Ovacık strike-slip faults coeval?; (v) what is the petrological meaning of the Kangal K-alkaline rocks? The answers to these questions may provide constraints on the reconstruction of the geodynamic evolution of the whole Central Eastern Anatolia Region.

Differentiation processes during ascent to surface

Before going through the discussion about the issues previously reported, the evaluation of the contribution of the differentiation processes occurred during the ascent of the magmas to surface should be investigated in detail, to understand the geochemical changes affecting the primary magmas. Indeed, the volcanic rocks from the Sivas–Malatya region, as a whole, show a large chemical compositional range, from olivine-bearing basalts to rhyolites, with MgO and SiO_2 ranging from 1.08 to 14.1 wt% and from 43.0 to 70.5 wt%, respectively (Fig. 4, ESM 4). This suggests that low-pressure differentiation processes played an important role in producing the compositional variability observed within each group of rocks in the region. Among the studied samples, only two from the Sivas volcanic field have geochemical and petrographic characteristics compatible

Table 4 Sr-Nd–Pb isotopes measured and age corrected for some selected samples

Sample	Unit	Rock type	Age (Ma)	Ref.	$^{87}Sr/^{86}Sr_m$	± 2σ	$^{87}Sr/^{86}Sr_i$	$^{143}Nd/^{144}Nd_m$	± 2σ	$^{143}Nd/^{144}Nd_i$	$^{206}Pb/^{204}Pb_m$	± 2σ	$^{206}Pb/^{204}Pb_i$	$^{207}Pb/^{204}Pb_m$	± 2σ	$^{207}Pb/^{204}Pb_i$	$^{208}Pb/^{204}Pb_m$	± 2σ	$^{208}Pb/^{204}Pb_i$
CA 41	Kangal	K-Trachy-andesite	5.27	1	0.704792	0.000010	0.70477	0.512693	0.000006	0.51269	18.6907	0.0031	18.683	15.6504	0.0026	15.650	38.8031	0.0063	38.790
CA 43	Kangal	Basalt	4.00	1	0.704254	0.000008	0.70425	0.512770	0.000008	0.51277	18.5268	0.0046	18.522	15.6352	0.0038	15.635	38.5866	0.0096	38.581
CA 44	Kangal	K-Trachy-andesite	5.11	2	0.705220	0.000006	0.70520	0.512627	0.000006	0.51262	18.6600	0.0005	18.655	15.6475	0.0005	15.647	38.8104	0.0012	38.804
CA 145	Kepez Dağ	Basalt	13.58–13.99	3	0.704670	0.000005	0.70465	0.512755	0.000004	0.51274	18.9439	0.0059	18.943	15.6753	0.0071	15.671	38.9771	0.0063	38.977
CA 146	Kepez Dağ	Dacite	13.58–15.39	4	0.705110	0.000011	0.70499	0.512610	0.000008	0.51260	18.7255	0.0048	18.718	15.6818	0.0039	15.681	38.8589	0.0099	38.851
CA 148	Kepez Dağ	Andesite	13.58–15.39	4	0.705466	0.000007	0.70539	0.512655	0.000008	0.51264	18.9435	0.0033	18.934	15.7120	0.0027	15.712	39.1516	0.0066	39.141
CA 48	Sivas	Basalt	13.97	2	0.705537	0.000006	0.70553	0.512624	0.000009	0.51261	19.1230	0.0053	19.105	15.7080	0.0043	15.707	39.2641	0.0107	39.238
CA 50	Sivas	Basanite	13.1–14.81	1	0.705537	0.000005	0.70552	0.512618	0.000010	0.51261	19.0644	0.0014	19.048	15.6821	0.0012	15.681	39.1495	0.0028	39.126
CA 53	Sivas	Basalt	15.71	2	0.704158	0.000008	0.70414	0.512840	0.000010	0.51282	18.9596	0.0027	18.953	15.6903	0.0022	15.690	39.0205	0.0056	39.013
CA 150	Arguvan	Basalt	15.58	2	0.703855	0.000009	0.70384	0.512855	0.000011	0.51284	18.9195	0.0014	18.914	15.6467	0.0011	15.646	38.9095	0.0029	38.902
CA 153	Arguvan	Mugearite	15.30	2	0.704380	0.000007	0.70432	0.512781	0.000021	0.51277	18.8732	0.0009	18.873	15.6703	0.0008	15.670	38.9425	0.0019	38.942
CA 154	Arguvan	Hawaiite	15.30	2	0.703476	0.000017	0.70347	0.512918	0.000010	0.51291	18.9949	0.0042	18.987	15.6610	0.0039	15.661	38.9813	0.0094	38.974
CA 158	Arguvan	Basalt	10.75	2	0.703652	0.000008	0.70365	0.512780	0.000010	0.51277	19.0198	0.0018	19.020	15.6622	0.0005	15.662	38.9592	0.0036	38.959
CA 156	Yamadağ	Andesite	13.61–15.90	5	0.704002	0.000008	0.70396	0.512880	0.000013	0.51287	18.8846	0.0006	18.885	15.6644	0.0010	15.664	38.9386	0.0039	38.939

(1) Platzman et al. (1998); (2) this study; (3) Ekici (2016); (4) Gürsoy et al. (2011); (5) Ekici et al. (2007)

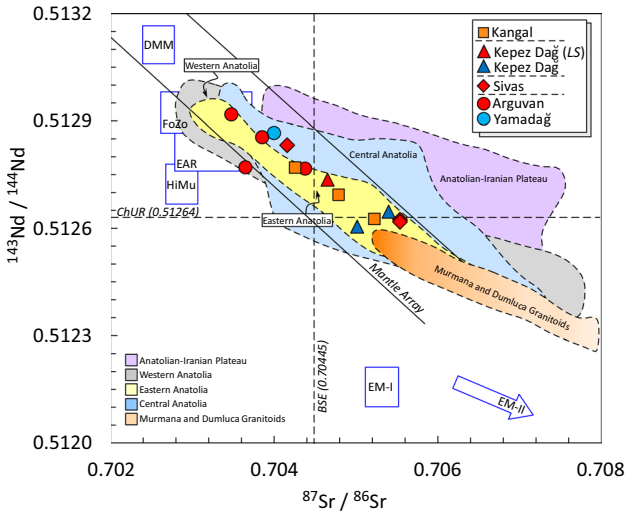

Fig. 6 $^{143}Nd/^{144}Nd_i$ vs. $^{87}Sr/^{86}Sr_i$ isotopic ratios for the studied rocks; BSE is the Bulk Silicate Earth; ChUR is the Chondritic Uniform Reservoir. Mantle end-members are also reported: DMM (Depleted Morb Mantle) from Workman and Hart (2005); EAR (European Asthenospheric Reservoir) from Cebriá and Wilson (1995); FoZo (Focal Zone), HiMu = High μ ($\mu = {}^{238}U/{}^{204}Pb$ ratio), EM-I (Enriched Mantle I), and EM-II (Enriched Mantle II) from Zindler and Hart (1986)

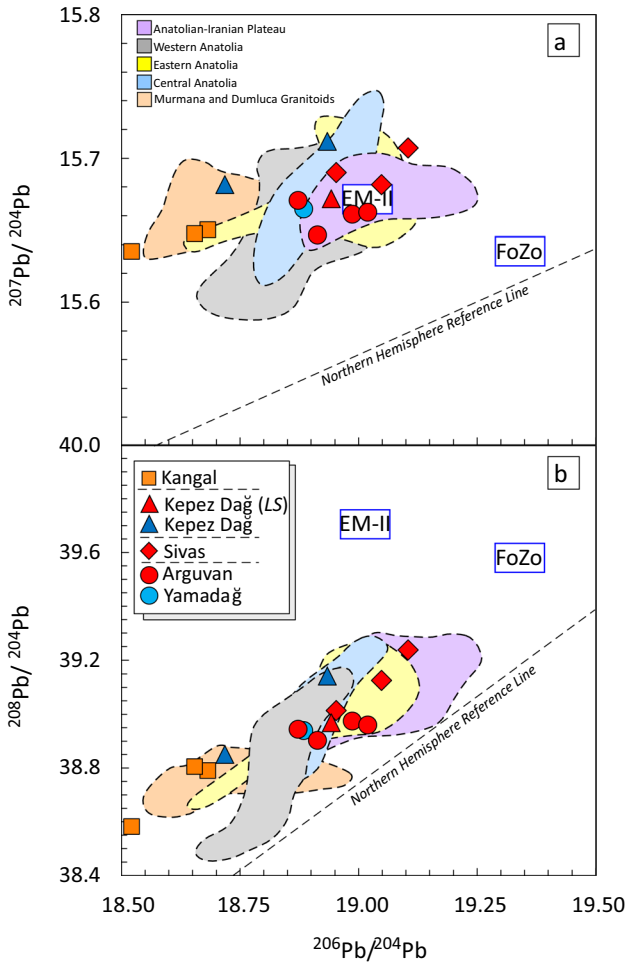

Fig. 7 **a** $^{207}Pb/^{204}Pb_i$ vs. $^{206}Pb/^{204}Pb_i$ and **b** $^{208}Pb/^{204}Pb_i$ vs. $^{206}Pb/^{204}Pb_i$ diagrams. Dashed line represents the Northern Hemisphere Reference Line (NHRL, after Hart, 1984). Mantle end-members as in Fig. 6

with primary mantle melts (e.g., Mg# > 70; Niu and O'Hara 2008), whilst all of the other samples had suffered significant crystal fractionation, crustal contamination and/or a combination of both processes. The crustal contamination might be also responsible for the large variability in radiogenic isotope compositions (Figs. 6 and 7).

In rocks from Kepez Dağ, Yamadağ volcanic complex, and Kangal volcanic field (Figs. 8) radiogenic isotopes, and in particular $^{87}Sr/^{86}Sr_i$, covary strictly with MgO and SiO_2 contents. This suggests that fractional crystallization alone is insufficient to explain the differentiation process affecting most of the volcanic rocks from Sivas–Malatya region.

The simultaneous decrease of CaO, Fe_2O_3, MnO and V with the decrease of MgO observed among calc-alkaline volcanic rocks of the Yamadağ and Kepez Dağ indicates a role of olivine and clinopyroxene fractionation during their differentiation (Fig. 4 and Fig. ESM 5a). Besides, plagioclase fractionation is supported by the positive correlation between CaO/Al_2O_3 and Sr with MgO. Crustal contamination is also needed to completely explain the Sr-isotopic variability observed (Fig. 8a, b).

To better constrain the differentiation model among the calc-alkaline volcanic rocks of Yamadağ and Kepez Dağ volcanic complexes we applied an integrated approach using both the XLFRAC code (Stormer and Nicholls 1978), for modelling major elements and the Energy-Constrained Assimilation-Fractionation Crystallization code (i.e. EC-AFC; Spera and Bohrson 2001), for trace elements and isotopes. Regarding the latter, it is important to note that, even if the integration of thermal energy, species and mass conservation into simulations of AFC processes in complex magmatic systems is performed with the EC-AFC model, this requires tightly constrained input parameters, which may be well-known in a single magma plumbing system, which is not the case for Yamadağ and Kepez Dağ volcanic complexes. In these cases, the result of the modeling must be considered semi-quantitative estimates. The end members used for the modelling were the most primitive samples of each series, as starting values (ESM 6), and the Upper Cretaceous Murmana granitoid from Divriği-Sivas region (sample MMG1; Boztuğ et al. 2007), as continental crustal contaminant.

The XLFRAC results are (i) 62–64 vol% of crystal mass removal, with an assemblage consisting of clinopyroxene (49 vol%) + plagioclase (44 vol%) + magnetite (7

vol%), associated to the digestion of 8 vol% of assimilated continental crust for the Yamadağ volcanic complex, and (ii) similar crystal mass removal, with an assemblage consisting of plagioclase (54 vol%) + clinopyroxene (36 vol%) + amphibole (6 vol%) + magnetite (4 vol%), associated to an assimilation of 11 vol% of continental crustal material for the Kepez Dağ volcanic complex. The XLFRAC code, when resting on coherent petrologic and mineralogical constraints, is the best approximate to describe major element variation, however, it does not take into account any change in fractionation assemblage, a chemical variation of fractionating phases or any energy balance (e.g., the heat supplied by magma and the latent heat of crystallization should be equal to the heat necessary to trigger melting of the mineral phases of the assimilant). Therefore, for trace elements, we applied the EC-AFC model, keeping in mind the limits deriving from the uncertainty on some thermochemical parameters. Thermal and compositional parameters are listed in detail in ESM 6, and results for Sr, Rb and $^{87}Sr/^{86}Sr$ isotope ratio are plotted in Fig. 9. According to the EC-AFC model outputs the calc-alkaline magmas can be explained by ≈ 65 to 74% fractional crystallization and up to 10–20% crustal digestion for the Yamadağ and Kepez Dağ volcanic complexes, respectively ($R \approx 0.15$ to 0.20). The good agreement between the results of the XLFRAC and EC-AFC suggests that the observed compositional spread of magmas from both calc-alkaline volcanic complexes of the region is due to a combination of crystal fractionation plus crustal assimilation at crustal depths.

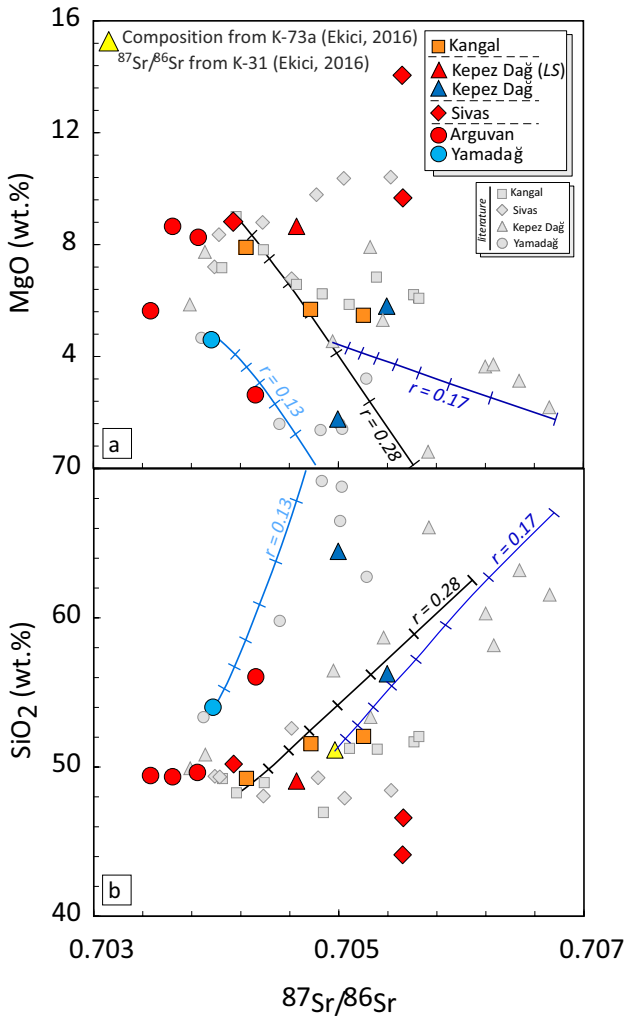

Fig. 8 MgO vs. $^{87}Sr/^{86}Sr_i$ (**a**) and SiO_2 *vs.* $^{87}Sr/^{86}Sr_i$ (**b**) diagram. AFC trajectories are drawn taking into account results from XLFRAC modelling for major elements, and AFC equations of DePaolo (1981) for elemental and isotopic Sr values. Full calculations and parameters in ESM 6 and ESM 8. Dots on the curve represent 10% Fractional crystallization steps

On the other hand, the Na-alkali basaltic rocks from Sivas, Arguvan, and Kangal volcanic fields have Mg# between 55 and 66, except two samples from Sivas (Mg# = 72). Thus, also most of these rocks do not represent magmas on the liquidus of a mantle source. Also in these cases, olivine was found to be a fractionating phase, the only one in the first stage of evolution, whereas clinopyroxene and plagioclase joined the fractionation assemblage later (MgO < 8 wt%). Volcanic rocks from Sivas and Arguvan volcanic fields are characterised by the positive correlation of Fe_2O_3, CaO, and MnO when plotted vs. MgO. The same is true for Ni, Cr, and Co. Neither crustal contamination nor magma mixing at a shallow level were recognised to have played significant roles in the isotopic variability, if any, of Na-alkaline volcanic rocks of Arguvan and Sivas volcanic fields. In the latter case, the $^{87}Sr/^{86}Sr$ increase with increasing MgO is simply the opposite of what is expected if the assimilation of crustal material occurred (Fig. 8). In summary, the Sr–Nd–Pb isotopic characteristics of Na-alkaline rocks from this region may be interpreted as a primary characteristic associated with their mantle source in spite of the differentiation processes affected these rocks as also found elsewhere (Casalini et al. 2017, 2018).

The same does not hold true for the K-alkaline rocks from Kangal volcanic field. The Kangal rocks show positive correlations of compatible elements when plotted *vs.* MgO, suggesting fractionation of olivine and clinopyroxene during differentiation associated with steep increases of incompatible and crustal-enriched elements (Fig. ESM 5a), which will correlate with the regular increase of Sr isotopes (Fig. 8). When modelled with XLFRAC, the variations observed in Kangal rocks are best described by a smaller amount of crystal fractionation with respect to the calc-alkaline rocks (crystal mass removed 35 vol%), with an assemblage made of clinopyroxene (51 vol%) + plagioclase (31 vol%) + olivine (15 vol%) + magnetite (4 vol%), with a total of 10 vol% of assimilated material (ESM 6).

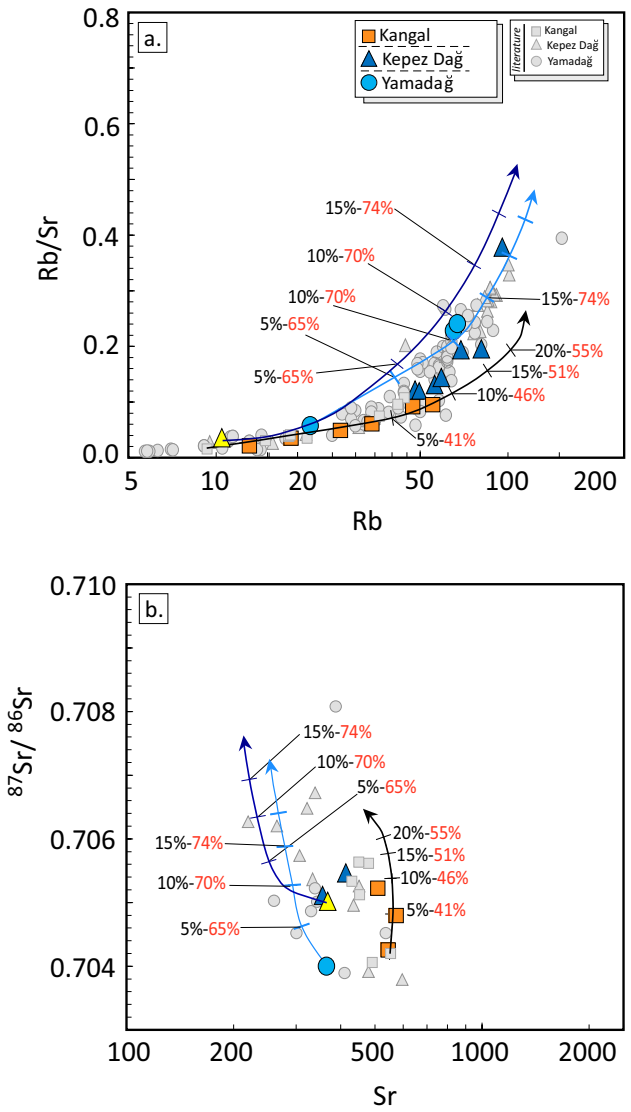

Fig. 9 Rb *vs.* Rb/Sr (**a**) and Sr *vs.* $^{87}Sr/^{86}Sr_i$ (**b**) diagrams of studied rocks, along with trajectories of EC-AFC modelling (Full calculations and Thermo-chemical parameters in ESM 6). The calc-alkaline rocks suites were modeled using thermal parameters of the "standard upper crust" (Bohrson and Spera 2001), and initial temperature of 450 °C for the assimilant. The K-alkaline suite was modeled using the "standard lower crust" and an assimilant initial temperature of 650 °C. Black numbers indicate % of assimilated mass, red numbers % of fractionated mass at the same level. It has to be noticed that in EC-AFC modeling some steps of Fractional Crystallization alone take place to provide the heat necessary to trigger melting of assimilant, roughly corresponding to 16% (Kangal), 46% (Yamadağ) and 49% (Kepez Dağ) for the three suites. This has been evidenced in Fig. 8a with corresponding labels., but not in Fig. 8b, given that Kd of Sr is very close to 1, then Sr content as well as $^{87}Sr/^{86}Sr$ are constant when fractional crystallization only takes place

Using EC-AFC algorithm Kangal K-alkaline rocks were derived by ≈ 51 vol% fractional crystallization and 15 vol% of assimilation of crustal lithologies with an $R \approx 0.29$. The enrichment in K related to crustal assimilation is a peculiar feature of these rocks, which is different from other potassic to ultrapotassic alkaline rocks found, although rarely, in the Anatolia volcanic region (Francalanci et al. 1990; Innocenti et al. 2005; Agostini et al. 2010a). The K-alkaline rocks from Western and Central Anatolia are associated to calc-alkaline high-Mg andesites (Agostini et al. 2005) and the K enrichment is generally a primary characteristic derived either directly from a metasomatised source mantle (Francalanci et al. 2000) or by the interaction between Na-alkaline sub-slab melts (intraplate-type affinity) with residual slab fluids (Agostini et al. 2007). Kangal volcanic rocks are characterised by low fluid-mobile/fluid-immobile element ratios (e.g. Rb/Nb ~ 1.5; Ba/Nb ~ 14) that help to exclude a significant contribution of slab component in their genesis. In summary, according with the modelling the enrichments in incompatible elements for Kangal suite (such as K and Pb; Fig. 4) are not a primary character of the mantle source but differentiation within the continental crust significantly modified original within-plate Na-alkaline magmas.

Insights into the nature of the Mantle Source

Patterns of the incompatible elements normalised to the concentrations of the Primitive Mantle (Fig. 4) are an important tool for deciphering at a glance the origin of the magmas and their possible relationships with the mantle geochemistry and the geodynamic setting (Hofmann 1997). The most valuable information is obtained when primitive mantle magmas are plotted, but knowing the extension of the differentiation process after magma genesis is helpful to filter the data to get backward to achieve information on the nature of the mantle sources, and the possible interactions between magmas deriving from consistently different reservoirs (e.g., Conticelli and Peccerillo 1992; Conticelli et al. 2002, 2013, 2015; Avanzinelli et al. 2009). To filter the data for shallow level differentiation processes when considering the Yamadağ, Kepez Dağ, and Kangal volcanic rocks, we only referred to the most primitive rocks from each group, discarding samples with $SiO_2 > 57$ wt% and $MgO < 4$ wt% for the calc-alkaline rocks, and with $SiO_2 > 52$ wt% and $MgO < 8$ wt% for the alkaline ones. Nonetheless, multi-element variation diagrams (Fig. 4) of the volcanic rocks of Sivas–Malatya region show significant differences among patterns of the different volcanic suites, arguing for different mantle sources for calc-alkaline, Na- and K-alkaline groups. This is also supported by the radiogenic isotope variations recorded in the most primitive terms (Fig. 8a, b).

Depletion of HFS elements, and in particular of Nb and Ta, with respect to LIL elements is attributed to subduction-related metasomatism (Tatsumi et al. 1986; Pearce 1982), therefore, we used the Ta/Yb vs. Th/Yb diagram (Fig. 10) to distinguish between rocks from slab-derived metasomatised

mantle sources from those with a within-plate origin. The rocks of Yamadağ and Kepez Dağ volcanic complexes fall well within the field of subduction-related volcanic rocks (Fig. 10). In addition, the large variability of $^{87}Sr/^{86}Sr$ (0.70396–0.70539), observed among the most primitive rocks of Yamadağ and Kepez Dağ, which are believed to have suffered no or very little crustal contamination, speaks for a mantle source modified by subduction-related metasomatic components (Francalanci et al. 1993; Elliott et al. 1997; Avanzinelli et al. 2012).

Primitive Na- and K-alkaline volcanic rocks from the Sivas, the Arguvan, and the Kangal volcanic fields fall close or within the Mantle Array (Fig. 10), but well distinct from each other.

The rocks from Sivas volcanic field define a trend partially deviating from the mantle array (Fig. 10) suggesting the occurrence of a heterogeneous mantle source possibly contaminated with some but a minor subduction-related component. This is also confirmed by the significant variations of Sr–Nd–Pb isotopic composition (Table 4), which is not related to the assimilation of upper crustal materials. Interestingly, volcanic rocks from Sivas define an array between two end-members: a basanitic and a basaltic one, with the latter enriched in incompatible trace elements and in radiogenic Sr isotope ($^{87}Sr/^{86}Sr = 0.70552$), showing also a higher Th/Yb = 4.53 (Fig. 10).

The Na-alkaline basalts from Arguvan, compared with the older Sivas volcanic rocks, are characterised by lower values of Th/Yb, Ta/Yb and $^{87}Sr/^{86}Sr$ ratios. Indeed, the Arguvan basalts show the lowest $^{87}Sr/^{86}Sr$ (0.70347–0.70432) and the highest $^{143}Nd/^{144}Nd$ (0.51277–0.51291) of the all volcanic rocks of the Sivas–Malatya region, which together with the $^{206}Pb/^{204}Pb$ values (18.91–19.02) are typical of depleted asthenosphere (Zindler and Hart 1986; Salters and Stracke 2004). On the other hand, the Th/Yb vs. Ta/Yb diagram (Fig. 10) splits these rocks into two clusters, characterised by similar Th/Yb but different Ta/Yb ratios, suggesting different conditions of pressure, temperature and/or melting degree.

The Kangal volcanic rocks, the youngest ones of the Sivas–Malatya region, are characterised by the highest Ta/Yb and Th/Yb values (Fig. 10), resembling those observed for typical OIB-like magmas. These rocks can be also clearly distinguished from the older Na-alkali basalt suites being very $^{206}Pb^*$ depleted (Fig. 6). However, as shown before, in this group the effects of crustal assimilation during magma evolution are clearly visible.

In summary, we interpret the Na-alkaline volcanic rocks from Sivas–Malatya region as generated by an asthenospheric mantle source. Trace element ratios and isotope large variability are due either to mantle source heterogeneity or different degrees of partial melting. To shed some light on this issue we used the REE distribution modelling

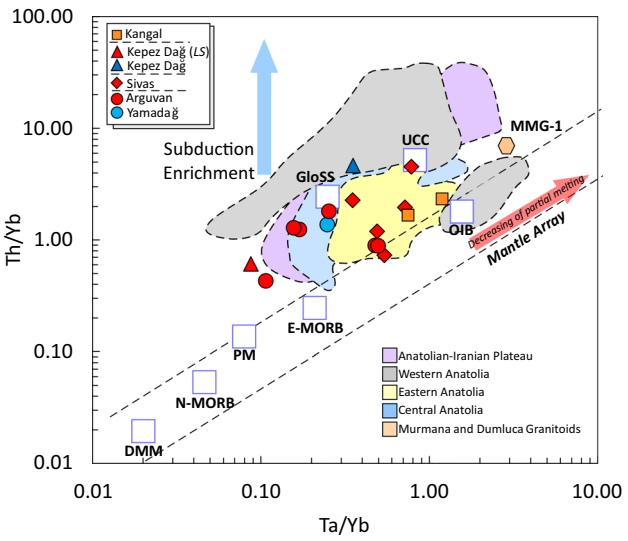

Fig. 10 Th/Yb vs. Ta/Yb (after Pearce 1982) diagram for the studied rocks. DMM (Depleted MORB Mantle) from Workman and Hart (2005); N-MORB (Normal MORB), PM (Primitive Mantle) E-MORB (Enriched MORB) and OIB from Sun and McDonough (1989); GloSS (Global Subducted Sediments) from Plank and Langmuir (1998); UCC (Upper Continental Crust) from and Taylor and McLennan (1985)

[i.e., $(Sm/Yb)_N$ vs. $(La/Sm)_N$] integrated with a thermobarometric estimation of magma segregation. The composition of the primordial mantle of Palme and O'Neill (2003) was chosen and then modelled through the non-modal batch melting algorithm (Shaw 1970). For estimating P–T segregation conditions, only primitive samples should be used, thus we selected only those with MgO > 8 wt% and SiO_2 < 52 wt%, with evidences of Fo-rich olivine on the liquidus. Then, we calculate back the primary magma compositions adding equilibrium olivine until magma equilibrates with olivine Fo_{90} (Pearce 1978), and calculating the composition of equilibrium olivine using $K_D\,(Fe/Mg)^{ol/liq} = 0.31$ (ESM 7). P and T were thus determined using a H_2O- and CO_2-rich system suggested by Plank and Forsyth (2016), which better approximates the intensive parameters of potential temperature and pressure for this type of magmas (ESM 7). According to this model, the Sivas basalt suite was generated by a partial melting degree of ≈ 2 to 4% in the spinel stability field, with a potential temperature of ≈ 1440 to 1490 °C and pressures of 17–26 kbar (Figs. 11 and 12). The Sivas basanitic suite shifted toward higher P (≈ 1493 °C and ≈ 29 kbar, respectively) at lower degrees of partial melting (≈ 1%) in the stability field of garnet (Figs. 11 and 12).

The middle-late Miocene Na-alkaline basalts from Arguvan define two trends in the $(Sm/Yb)_N$ vs. $(La/Sm)_N$ diagram, indicative of different conditions of partial melting.

Indeed, basalts emplaced in the Ortülü Pass area indicate potential T and P of ≈ 1384 to 1419 °C and ≈ 15.5 to 16.7 kbar, respectively, and fall within the garnet-free melting trajectory, with variable partial melting degrees (2–7%). Similar partial melting degrees (≈ 3.0 to 4.0%), as well as potential T and P (≈ 1401 to 1431 °C and 15.3–17.5 kbar, respectively) of melt segregation were found for samples from Arguvan and Arapgir areas, which show a detectable but very small amount of garnet in the source (Figs. 11 and 12).

Magmatism and tectonics

The present-day Anatolian microplate is the result of a complex geodynamic process that involved the subduction beneath the Eurasian plate of the oceanic lithospheres belonging to the Arabian and African plates. Eurasia and Arabia collided and sutured along the Bitlis Zagros Zone once the oceanic lithosphere was consumed completely (e.g., Şengör and Yılmaz 1981; Schildgen et al. 2014), forming, in Central and Eastern Anatolia, shortening and crustal thickening that led to the formation of the Anatolian-Iranian Plateau (e.g., Şengör et al. 2003). Subduction of the African oceanic lithosphere still persists at present only to the west of Cyprus, generating in Western Anatolia extensional tectonics related to the slab retreat of the Hellenic-Aegean slab. The segment of the African trench from Cyprus Island to the Dead Sea fault zone experienced incipient collision phases, leading to moderate thickening with the formation of uplands of more than 1000 m altitude, represented by the Central Anatolian Plateau (e.g., Schildgen et al. 2014). This motion is accommodated since the middle Miocene by the dextral Northern Anatolian Fault (Sengör and Gorür 1985) and its conjugate faults, and, subsequently, from the late Miocene to Pliocene, also by the sinistral Eastern Anatolian Fault (e.g. Bozkurt 2001). The Anatolian Fault Zone represents a wide area in which intracontinental strike-slip faults developed, and leading to the formation of several pull-apart basins (e.g., Di Giuseppe et al. 2017 and references therein) (Fig. 13).

In this geodynamic context, our interest focuses on the role played by the Cyprus slab in the tectonic development of the region. Recent studies of the Cappadocian volcanic region revealed that the fragmented Cyprus slab beneath Central Anatolia is located too deep (> 200 km) for causing recent (Pleistocene) volcanism in the region (Biryol et al. 2011; Reid et al. 2017). Furthermore, geophysical observations such as high plateau-like topography, slow seismic velocities beneath the upper mantle, high heat flow as well as lithospheric thinning testify the uprising of hot sub-lithospheric mantle responsible of the alkaline magmatism in Central Anatolia (Şengör and Yılmaz 1981; Gans et al. 2009; Govers and Fichtner 2016; Uluocak et al. 2016; Di Giuseppe

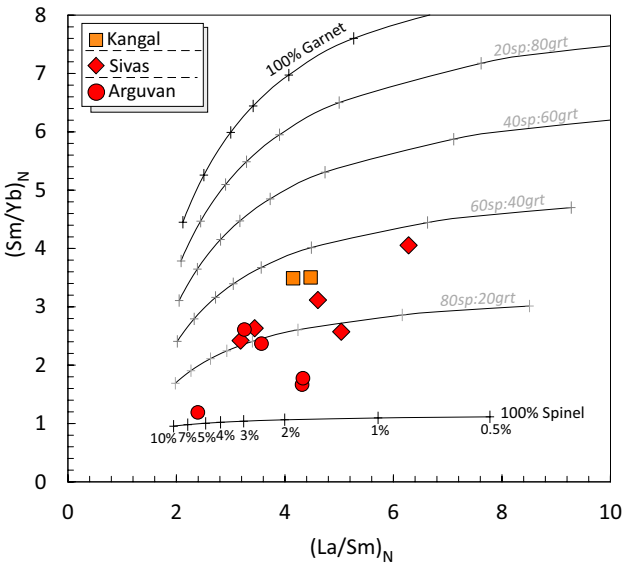

Fig. 11 $(Sm/Yb)_N$ vs. $(La/Sm)_N$ diagram for the studied rocks. No modal batch melting trajectories are drawn for garnet and spinel lherzolitic sources and normalised to PM (Primitive Mantle; Palme and O'Neill 2003). Mineral and melt modes of spinel and garnet peridotite sources are $ol_{.578(0.1)} + opx_{.27(0.27)} + cpx_{.119(0.5)} + sp_{.033(0.13)}$ and $ol_{.598(0.05)} + opx_{.211(0.2)} + cpx_{.076(0.3)} + gt_{.115(0.45)}$ respectively (Thirlwall et al. 1994). Partition coefficient and DMM compositions are reported in ESM 8

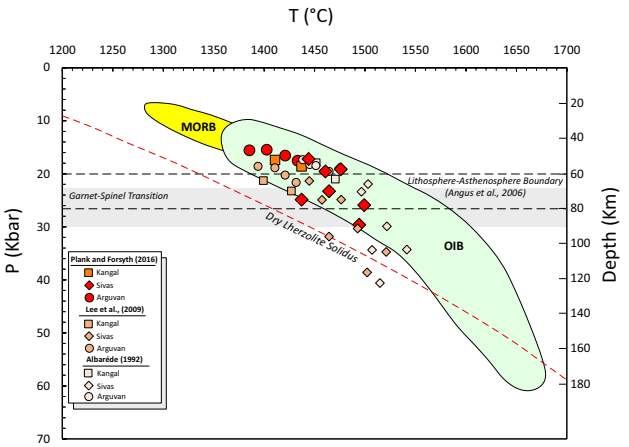

Fig. 12 Potential temperature and pressure calculated for selected primitive basaltic magma composition of the Sivas–Malatya region. Near-vertical lines represent solid mantle adiabats. Fields of MORB and OIB are from Lee et al. (2009). The lithosphere-asthenosphere boundary is located at about 60–80 km as constrained by geophysical data reported in Angus et al. (2006). Garnet and spinel transition zone after Fumagalli and Klemme (2015). H_2O content in the melt is estimated by fractionation correction of the Ce assuming Central Eastern Anatolia basalts have similar H_2O/Ce ratios as oceanic basalts (≈ 200; Herzberg et al. 2007). All the temperatures and pressures estimated from Albarède (1992), Lee et al. (2009), and Plank and Forsyth (2016) are presented in the diagram

et al. 2018; McNab et al. 2018). A recent study of Abgarmi et al. (2017) proposed that roll-back of the Cyprus slab started in the middle Miocene, favouring the onset of the volcanism in the Central Anatolia Volcanic Province. Actually, beneath this area, seismic anomalies reveal the presence of a sub-horizontal fragmented slab that favoured the upwelling of sub-lithospheric mantle (e.g., Reid et al. 2017).

In the Sivas–Malatya region, just located east of the Cappadocian Volcanic field, subduction-related calc-alkaline magmatic activity, here represented by the Yamadağ and Kepez Dağ volcanic complexes, took place in the early to middle Miocene time (19.5 and 13.6 Ma, respectively), during the subduction of the oceanic African slab, the Africa-Eurasia collision being marked by the 13 Ma emplacement of Bitlis-Zagros ophiolitic suture (Fig. 13a). We thus interpret the calc-alkaline Yamadağ and Kepez Dağ activity as the arc volcanism, like the contemporaneous Mazgirt volcanism taking place some 100 km to the east (Di Giuseppe et al. 2017; Agostini et al. 2019).

The 13 Ma collision and the onset of the Northern Anatolian Fault determined the main shift from compressional to strike-slip tectonics in Central Anatolia leading to the development or reactivation of transcurrent faults with the normal component. Examples are the late Miocene-early Pliocene Ecemiş and Tuz Gölü strike-slip faults in Cappadocia Volcanic field and the middle Miocene Kızılırmak fault in the Sivas region (e.g., Toprak 1994; Dirik et al. 1999). The oldest alkaline basalts of the region are those from Sivas basin (Fig. 13a), emplaced along the Kızılırmak fault during the early-middle Miocene time (16.7–13.1 Ma). These magmas formed at depths ranging between 92 and 53 km, from a heterogeneous mantle source, with a variable amount of garnet and spinel as Al-bearing phases and, probably, with some hydrous phases (Kürkçüoğlu et al. 2015). These alkali basalts have some trace element and isotopic features, such as LILE/HFSE enrichments, $^{87}Sr/^{86}Sr > 0.7040$, different from typical OIB-intraplate alkali basalts found elsewhere in Western and Eastern Anatolia (Kula, Innocenti et al. 2005, Elazığ, Di Giuseppe et al. 2017), and similar to alkali basalts outcropping just to the west and to the east of the study area, such as those of Cappadocia (Di Giuseppe et al. 2018), Tunceli (Agostini et al. 2019) and Karlıova-Varto (Karaoğlu et al. 2020), which still retain a weak imprint of mantle modified by subduction-related metasomatism. Sivas basalts, as well as the first pulse of Arguvan basalts, along with those of Galata Massif (Keller et al. 1992; Wilson et al. 1997; Varol et al. 2014) predate the Bitlis-Zagros collision. This supports the hypothesis of an older activity of the North Anatolian Shear Zone, with its conjugate structures (e.g., Ottria et al. 2017). It is noteworthy that Sivas alkali basalts are contemporaneous with the arc volcanism of Yamadağ and Kepez Dağ volcanic complexes, occurring only 50–100 km to the southeast.

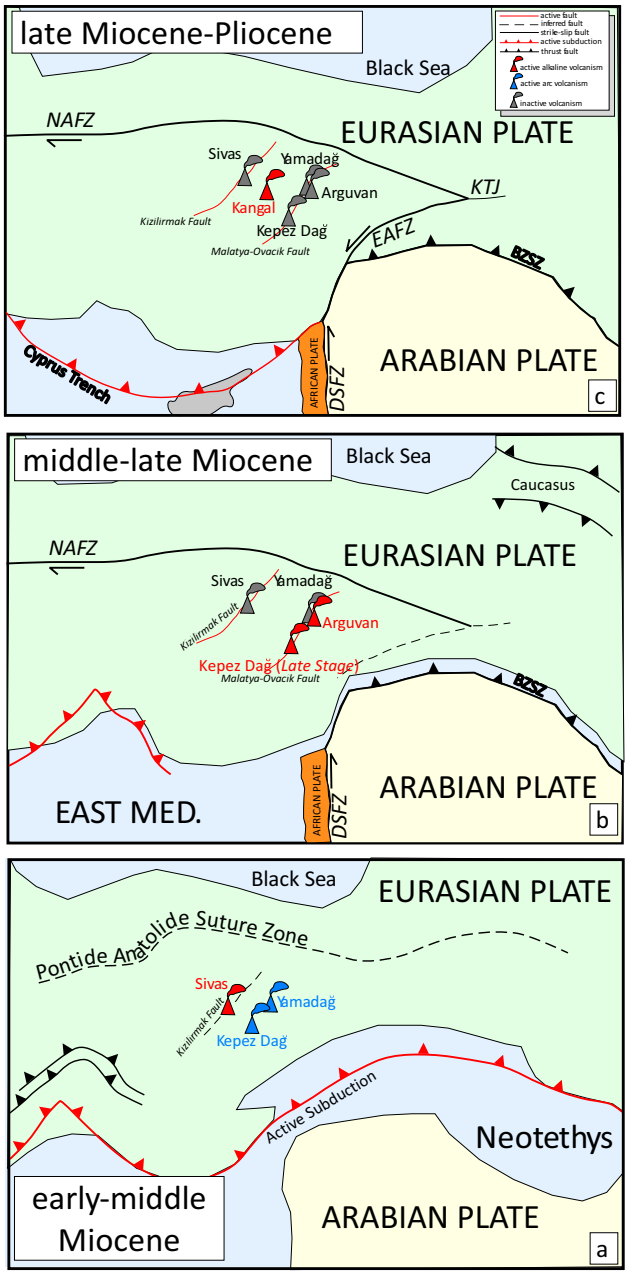

Fig. 13 Simplified geodynamic evolution of the Sivas–Malatya region (modified after Agostini et al. 2019); **a** early-middle Miocene magmatic activity in the Yamadağ, Kepez Dağ, and Sivas cluster; **b** middle Miocene volcanism in the Arguvan area (Arguvan, Arapgir, and Ortülü Pass); **c** late Miocene–Pliocene volcanism within the Kangal basin. *NAFZ* North Anatolian Fault Zone, *EAFZ* East Anatolia Fault Zone, *DSFZ* Dead Sea Fault Zone, *KTJ* Karlıova Triple Junction, *BZSZ* Bitlis-Zagros Suture Zone

Alkali basalts of Arguvan are partially coeval with the calc-alkaline volcanic activity of the Yamadağ, with several basaltic lavas, occurring in Arapgir (12.2–15.8 Ma; Arger et al. 2000; Kürüm et al. 2008), and Ortülü Pass (15.8 Ma), and in Arguvan (10.9–10.6 Ma), along or very close to

the Malatya-Ovacık strike-slip fault (Fig. 13b). More to the south, scarce alkali basalts are also found at the top of the Kepez Dağ volcanic sequence, aged 13.6–13.9 Ma (Ekıcı 2016). All of these alkali basalts are similar, both in age and composition to the transitional basalt of Tunceli (11.4–11.0 Ma; Di Giuseppe et al. 2017; Agostini et al. 2019).

The last phase of activity in the study area occurred at the end of Miocene and during the Pliocene time in the Kangal Basin (5.9–4.0 Ma, Fig. 13c). These basalts have the typical characters of intraplate OIB-type alkali basalts, even if they show mostly a K- rather than a Na- affinity, mostly because assimilation of crustal material overprinted their original characters. Noteworthy, they are very similar in age and petrologic characters to Karakoçan lavas outcropping in Tunceli-Bingöl provinces (100–150 km to the east).

Conclusions

In this study, we present new geochemical, petrological, isotopic and geochronologic data of early Miocene to Pliocene volcanic activity developed in the Sivas-Malaya region (Central Eastern Anatolia). Data allowed us to distinguish four main phases of magmatic activity, with emplacement of magmas with different geochemical and isotopical characteristics:

(a) *Yamadağ and Kepez Dağ volcanic complexes* calc-alkaline volcanic rocks, which vary in composition from basalts to rhyolites, were emplaced during the early and middle Miocene time in the Yamadağ (19.5–13.6 Ma) and Kepez Dağ (16.3–14.1 Ma) volcanic complexes. These rocks are characterised by the typical geochemical and isotopical features of arc-related volcanism, including marked enrichment in LILE/HFSE ratios, and relatively high $^{87}Sr/^{86}Sr$ (0.70396–0.705539) and low $^{144}Nd/^{143}Nd$ (0.51260–0.51287), indicating that these magmas were sourced in a mantle wedge modified by recycled sediments. Evolution of these rocks is driven by crystal fractionation of a gabbroic assemblage with a significant amount of crustal contamination, which is more pronounced in the Kepez Dağ. These products represent the volcanic arc linked with subduction of the African oceanic lithosphere.

(b) *Sivas volcanic field* contemporaneously, monogenetic Na-alkaline basanitic and basaltic magmatic activity developed in the Sivas volcanic field, along the Kızılırmak strike-slip fault, during the early-middle Miocene (16.7–13.1 Ma). Our K–Ar and ^{40}Ar–^{39}Ar data are well within the radiometric ages available in literature and range from 15.7 to 14.0 Ma. These samples are characterised by a variable degree of LILE enrichments and HFSE depletions, negative anomalies in Nb–Ta–Ti in primitive-mantle normalised patterns, variable $^{87}Sr/^{86}Sr$ ratios (0.7041–0.7055) and $^{144}Nd/^{143}Nd$ (0.51261–0.51282), revealing the occurrence of some interaction with slab-modified mantle. All these characteristics reflect the occurrence of two different end members occurring in a heterogeneous mantle source located at depths of 53–92 km;

(c) *Arguvan volcanic field* Na-alkaline basaltic to hawaiitic rocks were emplaced starting from the middle Miocene (15.3 Ma) in the Arguvan area. The magmatic activity continued through the late Miocene both in the Arguvan (10.9 Ma; Reid et al. 2019), and Arapgir areas (12.2–8.9 Ma; Kürüm et al. 2008). Our age determinations point out that activity in the area around Ortülü Pass is also late Miocene in age (10.6 Ma). Na-alkaline rocks from Arguvan are less enriched in incompatible elements with respect to the Na-alkaline rocks from Sivas, and they have even smaller negative anomalies at Nb and Ta. These rocks few postdate the calc-alkaline activity of Yamadağ, and are similar, in age and geochemistry, to some alkali basalts found on the top of Kepez Dağ volcanic succession. Their radiogenic isotope ratios (e.g. $^{87}Sr/^{86}Sr \approx 0.70365$–$0.70432$) overlap the Na-alkaline rocks emplaced in Kula (Western Anatolia), Kızılırmak and Acıgöl-Nevşehır (Cappadocia), and Elazığ (Eastern Anatolia);

(d) *Kangal volcanic field* K-alkaline rocks ranging from basalts to shoshonites, emplaced in the southwestern sector of the study area, in the Kangal Basin, during the late Miocene to Pliocene (5.9–4.0 Ma). In this case, our K–Ar data are coherent to those reported in the literature, ranging from 5.1 to 4.8 Ma. Major and trace element abundances are those of the typical OIB magmas. The high $^{87}Sr/^{86}Sr$ (0.70425–0.70520), as well as the Nb–Ta negative anomalies, and the K and Pb enrichments are related to various degree of crustal contamination of magmas derived from mantle source not affected by subduction components.

It is noteworthy that, in the study area, during the early to middle Miocene we have two different kinds of activity: (i) to the north-west, in the Sivas basin, Na-alkaline volcanism along the strike-slip Kızılırmak fault, a conjugate fault of the North Anatolian Shear Zone. This activity, along with the alkali basalts of the Galatia Volcanic Province witnesses the possible development of strike-slip tectonics in this area before the Arabia-Eurasia collision (~ 13 Ma); (ii) to the south-east, the calc-alkaline activity of Yamadağ and Kepez Dağ. These products represent the volcanic arc linked with subduction of the African oceanic lithosphere.

The end of calc-alkaline activity is marked by a partially coeval alkali basaltic volcanic phase, occurring at Arguvan

along the Malatya-Ovacik strike-slip fault at 15–9 Ma. Another phase of alkali basaltic volcanism developed within Kangal basin during the late Miocene to Pliocene.

Supplementary Information The online version contains supplementary material available at https://doi.org/10.1007/s00531-021-01995-0.

Acknowledgements The authors thank Z. Pecskay (MTA-Atomki, Debrecen, Hungary) and M. D'Orazio (DST-University of Pisa, Italy) for K–Ar ages and ICP-MS data, respectively, A. Rielli and S. Vezzoni for constructive criticism and discussion. A professional proofreading service reviewed the English style and grammar of the manuscript. We acknowledge two anonymous reviewers and the Editor in Chief, Wolf-Christian Dullo, whose constructive comments improved the quality of the manuscript.

Funding Financial support was provided by IGG-CNR-P0000514 funds with S. Agostini as PI, by PRIN-2015 (Grant# 20158A9CBM) with S. Conticelli as PI, and PRIN-2017 (Grant#2017BX42Z) with G. Di Vincenzo as PI.

References

Abgarmi B, Delph JR, Ozacar AA, Beck SL, Zandt G, Sandvol E, Turkelli N, Biryol CB (2017) Structure of the crust and African slab beneath the central Anatolian plateau from receiver functions: new insights on isostatic compensation and slab dynamics. Geosphere 13:1774–1787. https://doi.org/10.1130/GES01509.1

Adıyaman Ö, Chorowicz J, Arnaud ON, Gündogdu MN, Gourgaud A (2001) Late Cenozoic tectonics and volcanism along the North Anatolian Fault: new structural and geochemical data. Tectonophysics 338:135–165. https://doi.org/10.1016/S0040-1951(01)00131-7

Agard P, Omranı J, Jolivet L, Whitechurch H, Vrielynck B, Sparkam W, Monié P, Meyer B, Wortel R (2011) Zagros orogeny: a subduction-dominated process. Geol Mag 148:692–725. https://doi.org/10.1017/S001675681100046X

Agostini S, Doglioni C, Innocenti F, Manetti P, Savasçın MY, Tonarini S (2005) Tertiary high-Mg volcanic rocks from Western Anatolia and their geodynamic significance for the evolution of the Aegean area. In: Fytikas M, Vougioukalakis GE (eds) The South Aegean Active Volcanic Arc. Elsevier Book Spec Series, Develop Volcanol 7, pp 345–362

Agostini S. Doglioni C, Innocenti F, Manetti P, Tonarini S, Savasçın MY (2007) The transition from subduction-related to intraplate Neogene magmatism in the Western Anatolia and Aegean area. In: Beccaluva L, Bianchini G, Wilson M (eds) Cenozoic Volcanism in the Mediterranean Area. Geol Soc Am Spec Pap, vol 418, pp 1–15. https://doi.org/10.1130/2007.2418(01)

Agostini S, Tokçaer M, Savaşçın MY (2010a) Volcanic rocks from Foça-Karaburun and Ayvalık-Lesvos Grabens (Western Anatolia) and their petrogenic-geodynamic significance. Turk J Earth Sci 19:157–184. https://doi.org/10.3906/yer-0905-11

Agostini S, Doglioni C, Innocenti F, Manetti P, Tonarini S (2010b) On the geodynamics of the Aegean rift. Tectonophysics 488:7–21. https://doi.org/10.1016/j.tecto.2009.07.025

Agostini S, Savaşçın MY, Di Giuseppe P, Di Stefano F, Karaoğlu Ö, Lustrino M, Manetti P, Ersoy Y, Kürüm S, Öztufekçi Önal A (2019) Neogene volcanism in Elaziğ-Tunceli area (eastern Anatolia): geochronological and petrological constraints. Ital J Geosci 138:435–455. https://doi.org/10.3301/IJG.2019.18

Albarède F (1992) How deep do common basaltic magmas form and differentiate? J Geophys Res 97:10997–11009. https://doi.org/10.1029/91JB02927

Aldanmaz E (2002) Mantle source characteristics of alkali basalts and basanites in an extensional intracontinental plate setting, Western Anatolia, Turkey: implications for multi-stage melting. Int Geol Rev 44:440–457. https://doi.org/10.2747/0020-6814.44.5.440

Alıcı Şen P, Temel A, Gourgaud A (2004) Petrogenetic modelling of Quaternary post-collisional volcanism: a case study of central and eastern Anatolia. Geol Mag 141:81–98. https://doi.org/10.1017/S0016756803008550

Angus DA, Wilson DC, Sandvol E, Ni JF (2006) Lithospheric structure of the Arabian and Eurasian collision zone in eastern Turkey from S-wave receiver functions. Geophys J Int 166:1335–1346. https://doi.org/10.1111/j.1365-246X.2006.03070.x

Arger J, Mitchell JG, Westaway RWC (2000) Neogene and Quaternary volcanism of southeastern Turkey. In: Bozkurt E, Winchester JA, Piper JDA (eds) Tectonics and magmatism in Turkey and its surrounding area, vol 173. Geol Soc London Spec Publ, pp 459–487. https://doi.org/10.1144/GSL.SP.2000.173.01.22

Avanzinelli R, Lustrino M, Mattei M, Melluso L, Conticelli S (2009) Potassic and ultrapotassic magmatism in the circum-Tyrrhenian region: significance of carbonated pelitic vs. pelitic sediment recycling at destructive plate margins. Lithos 113:213–227. https://doi.org/10.1016/j.lithos.2009.03.029

Avanzinelli R, Prytulak J, Skora S, Heumann A, Koetsier G, Elliott T (2012) Combined ^{238}U–^{230}Th and ^{235}U–^{231}Pa constraints on the transport of slab-derived material beneath the Mariana Islands. Geochem Cosmochim Acta 92:308–328. https://doi.org/10.1016/j.gca.2012.06.020

Avanzinelli R, Bianchini G, Tiepolo M, Jasim A, Natali C, Braschi E, Dallai L, Beccaluva L, Conticelli S (2020) Subduction-related hybridization of the lithospheric mantle revealed by trace element and Sr–Nd–Pb isotopic data in composite xenoliths from Tallante (Betic Cordillera, Spain). Lithos 352:105316. https://doi.org/10.1016/j.lithos.2019.105316

Biryol CB, Beck SL, Zandt G, Özacar AA (2011) Segmented African lithosphere beneath the Anatolian region inferred from teleseismic P-wave tomography. Geophys J Int 184:1037–1057. https://doi.org/10.1111/j.1365-246X.2010.04910.x

Boccaletti M, Manetti P (1988) The main unconformities and tectonic events in the Pontides. Boll Geofis Teor Appl 30:9–16

Bohrson WA, Spera FJ (2001) Energy-constrained open system magmatic process II: application of energy-constrained assimilation and fractional crystallization (EC-AFC) model to magmatic system. J Petrol 42:1019–1041. https://doi.org/10.1093/petrology/42.5.1019

Elliott T, Plank T, Zindler A, White W, Bourdon B (1997) Element transport from slab to volcanic front at the Mariana arc. J Geophys Res 102:14991–15019. https://doi.org/10.1029/97JB00788

Bozkurt E (2001) Neotectonics of Turkey—a synthesis. Geodin Acta 14:3–30. https://doi.org/10.1016/S0985-3111(01)01066-X

Boztuğ D, Harlavan Y, Arehart G, Satır M, Avcı N (2007) K-Ar age, whole-rock and isotope geochemistry of A-type granitoids in the Divriği-Sivas region, eastern-central Anatolia, Turkey. Lithos 97(1–2):193–218. https://doi.org/10.1016/j.lithos.2006.12.014

Casalini M, Avanzinelli R, Heumann A, de Vita S, Sansivero F, Conticelli S, Tommasini S (2017) Geochemical and radiogenic isotope probes of Ischia volcano, Southern Italy: constraints on magma chamber dynamics and residence time. Am Miner 102:262–274

Casalini M, Heumann A, Marchionni S, Conticelli S, Avanzinelli R, Tommasini S (2018) Inverse modelling to unravel the radiogenic isotope signature of mantle sources from evolved magmas: the case-study of Ischia volcano. Ital J Geosci 137:420–432

Cebriá JM, Wilson M (1995) Cenozoic mafic magmatism in Western/Central Europe: a common European asthenosphere reservoir? Terra Nova Abstr 7:162

Cebriá JM, López-Ruiz J, Carmona J, Doblas M (2009) Quantitative petrogenetic constraints on the Pliocene alkali basaltic volcanism of the SE Spain Volcanic Province. J Volcanol Geotherm Res 185:172–180. https://doi.org/10.1016/j.jvolgeores.2009.05.008

Conticelli S (1998) The effect of crustal contamination on ultrapotassic magmas with lamproitic affinity: mineralogical, geochemical and isotope datafrom the Torre Alfina lavas and xenoliths, Central Italy. Chem Geol 149:51–81. https://doi.org/10.1016/S0009-2541(98)00038-2

Conticelli S, Peccerillo A (1992) Petrology and geochemistry of potassic and ultrapotassic volcanism in central Italy: petrogenesis and inferences on the evolution of the mantle sources. Lithos 28:221–240. https://doi.org/10.1016/0024-4937(92)90008-M

Conticelli S, D'antonio M, Pinarelli L, Civetta L (2002) Source contamination and mantle heterogeneity in the genesis of Italian potassic and ultrapotassic volcanic rocks: Sr–Nd–Pb isotope data from Roman Province and Southern Tuscany. Mineral Petrol 74:189–222

Conticelli S, Avanzinelli R, Poli G, Braschi E, Giordano G (2013) Shift from lamproite-like to leucititic rocks: sr–Nd–Pb isotope data from the Monte Cimino volcanic complex vs. the Vico stratovolcano, Central Italy. Chem Geol 353:246–266

Conticelli S, Avanzinelli R, Ammannati E, Casalini M (2015) The role of carbon from recycled sediments in the origin of ultrapotassic igneous rocks in the Central Mediterranean. Lithos 232:174–196

Dallai L, Bianchini G, Avanzinelli R, Natali C, Conticelli S (2019) Heavy oxygen recycled into the lithospheric mantle. Sci Rep 9:1–7. https://doi.org/10.1038/s41598-019-45031-3

Davies JH, von Blanckenburg F (1995) Slab breakoff: a model of lithosphere detachment and its test in the magmatism and deformation of collisional orogens. Earth Planet Sci Lett 129:85. https://doi.org/10.1016/0012-821X(94)00237-S

DePaolo DJ (1981) Trace element and isotopic effects of combined wall rock assimilation and fractional crystallization. Earth Planet Sci Lett 53:189–202. https://doi.org/10.1016/0012-821X(81)90153-9

Di Giuseppe P, Agostini S, Lustrino M, Karaoğlu Ö, Savaşçın MY, Manetti P, Ersoy Y (2017) Transition from compression to strike-slip tectonics revealed by miocene-pleistocene volcanism west of the Karlıova Triple Junction (East Anatolia). J Petrol 58:2055–2087. https://doi.org/10.1093/petrology/egx082

Di Giuseppe P, Agostini S, Savaşçın MY, Manetti P, Conticelli S (2018) Sub-lithospheric origin of Na-alkaline and calc-alkaline magmas in a post-collisional tectonic regime: Sr–Nd–Pb isotopes in recent monogenetic volcanism of Cappadocia, Central Turkey. Lithos 316–317:304–322. https://doi.org/10.1016/j.lithos.2018.07.018

Dilek Y, Sandvol E (2009) Seismic structure, crustal architecture and tectonic of the Anatolian-African Plate Boundary and the Cenozoic Orogenic Belts in the Eastern Mediterranean Region. In: Murphy JB, Keppie JD, Hynes AJ (eds) Ancient orogens and modern analogues. Geol Soc London Spec Publ, vol 327, pp 127–160. https://doi.org/10.1144/SP327.8

Dirik K, Göncüoğlu MC, Kozlu H (1999) Stratigraphy and pre-Miocene tectonic evolution of the southwestern part of the Sivas Basin, Central Anatolia, Turkey. Geol J 34:303–319

Dogan-Kulahci GD, Temel A, Gourgaud A, Varol E, Guillou H, Deniel C (2018) Contemporaneous alkaline and calc-alkaline series in Central Anatolia (Turkey): spatio-temporal evolution of a post-collisional Quaternary basaltic volcanism. J Volcanol Geotherm Res 356:56–74. https://doi.org/10.1016/j.jvolgeores.2018.02.012

Doglioni C, Agostini S, Crespi M, Innocenti F, Manetti P, Riguzzi F, Savaşçın MY (2002) On the extension in western Anatolia and the Aegean sea. J Virt Expl 8:169–184. https://doi.org/10.3809/jvirtex.2002.00049

Duggen S, Hoernle K, van den Bogaard P, Garbe-Schonberg D (2005) Post-collisional transition from subduction- to intraplate-type magmatism in the westernmost mediterranean: evidence for continental-edge delamination of subcontinental lithosphere. J Petrol 46:1155–1201. https://doi.org/10.1093/petrology/egi013

Ekıcı T (2016) Collision-related slab break-off volcanism in the Eastern Anatolia, Kepez volcanic complex (TURKEY). Geodin Acta 28(3):223–239. https://doi.org/10.1080/09853111.2015.1121796

Ekıcı T, Alpaslan M, Parlak O, Temel A (2007) Geochemistry of the Pliocene basalts erupted along the Malatya-Ovacik fault zone (MOFZ), Eastern Anatolia, Turkey: implications for source characteristics and partial melting processes. Chem Erde Geoch 67:201–212. https://doi.org/10.1016/j.chemer.2006.01.007

Ekıcı T, Alpaslan M, Parlak O, Uçurum A (2009) Geochemistry of the Middle Miocene Collision-related Yamadağı (Eastern Anatolia) Calc-alkaline Volcanics, Turkey. Turk J Earth Sci 18:511–528. https://doi.org/10.3906/yer-0712-1

Ewart A (1982) The mineralogy and petrology of tertiary-recent orogenic volcanic rocks with a special reference to the andesitic-basaltic compositional range. In: Thorpe RS (ed) Andesites. Wiley, Chichester, pp 26–87

Faccenna C, Bellier O, Martinod J, Piromallo C, Regard V (2006) Slab detachment beneath eastern Anatolia: a possible cause for the formation of the North Anatolian fault. Earth Planet Sci Lett 242:85–97. https://doi.org/10.1016/j.epsl.2005.11.046

Francalanci L, Civetta L, Innocenti F, Manetti P (1990) Tertiary-Quaternary alkaline magmatism of the Aegean-Western Anatolian area: a petrological study in the light of new geochemical and isotopic data. In: Savaşçın MY, Eronat AH (eds) IESCA 1990, Proceed vol II, pp 385–396

Francalanci L, Taylor SR, McCulloch MT, Woodhead JD (1993) Geochemical and isotopic variations in the calc-alkaline rocks of Aeolian arc, southern Tyrrhenian Sea, Italy: constraints on magma genesis. Contrib Mineral Petrol 113:300–313. https://doi.org/10.1007/BF00286923

Francalanci L, Innocenti F, Manetti P, Savasçin MY (2000) Neogene alkaline volcanism of the Afyon-Isparta area, Turkey: petrogenesis and geodynamic implications. Mineral Petrol 70(3–4):285–312. https://doi.org/10.1007/s007100070007

Fumagalli P, Klemme S (2015) Mineralogy of the Earth. Phase transitions and mineralogy of the upper mantle. In: Schubert G (ed) Treatise of geophysics, vol 2. Elsevier, Oxford, pp 7–31

Gans CR, Beck SL, Zandt G, Biryol CB, Özacar AA (2009) Detecting the limit of slab break-off in Central Turkey: new high resolution *Pn* tomography results. Geophys J Int 179:1566–1572. https://doi.org/10.1111/j.1365-246X.2009.04389.x

Gençoğlu Korkmaz G, Asan K, Kurt H, Ganerod M (2017) 40Ar/39Ar geochronology, elemental and Sr–Nd–Pb isotope geochemistry of the Neogene bimodal volcanism in the Yükselen area, NW Konya (Central Anatolia, Turkey). J Afr Earth Sci 129:427–444. https://doi.org/10.31016/j.jafrearsci.2017.02.001

Govers R, Fichtner A (2016) Signature of slab fragmentation beneath Anatolia from full waveform tomography. Earth Planet Sci Lett 450:10–19. https://doi.org/10.1016/j.epsl.2016.06.014

Gürsoy H, Tatar O, Piper J, Koçbulut F, Akpınar Z, Huang B, Roberts AP, Mesci BL (2011) Palaeomagnetic study of the Kepezdağ and Yamadağ volcanic complexes, central Turkey: neogene tectonic escape and block definition in the central-east Anatolides. J Geod 51:308–326. https://doi.org/10.1016/j.jog.2010.07.004

Hart SR (1984) A large-scale isotope anomaly in the Southern Hemisphere mantle. Nature 309:753–757. https://doi.org/10.1038/309753a0

Hawkesworth CJ, Gallagher K (1993) Mantle hotspots, plumes and regional tectonics as causes of intraplate magmatism. Terra Nova 5:552–559. https://doi.org/10.1111/j.1365-3121.1993.tb00304.x

Herzberg C, Asimow PD, Arndt NT, Niu Y, Lesher CM, Fitton JG, Cheadle MJ, Saunders AD (2007) Temperatures in ambient mantle and plumes: constraints from basalts, picrites and komatiites. Geochem Geophys Geosyst 8:1–34. https://doi.org/10.1029/2006GC001390

Hofmann AW (1997) Mantle geochemistry: the message from oceanic volcanism. Nature 385:219–229. https://doi.org/10.1038/385219a0

Innocenti F, Mazzuoli G, Pasquarè F, Radicati Di Brozolo F, Villari L (1975) The Neogene calcalkaline volcanism of Central Anatolia: geochronological data on Kayseri-Niğde area. Geol Mag 112:349–360. https://doi.org/10.1017/S0016756800046744

Innocenti F, Agostini S, Di Vincenzo G, Doglioni C, Manetti P, Savaşçın MY, Tonarini S (2005) Neogene and Quaternary volcanism in Western Anatolia: magma sources and geodynamic evolution. Mar Geol 221:397–421. https://doi.org/10.1016/j.margeo.2005.03.016

Irvine TN, Baragar WRA (1971) A guide to the chemical classification of the common volcanic rocks. Can J Earth Sci 8:523–548. https://doi.org/10.1139/e71-055

Karaoğlu Ö, Gülmez F, Göçmengil G, Lustrino M, Di Giuseppe P, Manetti P, Savaşçın MY, Agostini S (2020) Petrological evolution of Karlıova-Varto volcanism (Eastern Turkey): magma genesis in a transtensional triple-junction tectonic setting. Lithos 364–365:105524. https://doi.org/10.1016/j.lithos.2020.105524

Kaymakcı N, Aldanmaz E, Langereis C, Spell TL, Gurer OF, Zanetti KA (2007) Late Miocene transcurrent tectonics in NW Turkey: evidence from palaeomagnetism and ^{40}Ar–^{39}Ar dating of alkaline volcanic rocks. Geol Mag 144(2):379–392. https://doi.org/10.1017/S0016756806003074

Keller J, Jung D, Eckhardt FJ, Kreuzer H (1992) Radiometric Ages and Chemical Characterization of the Galatean Andesite Massif, Pontus, Turkey. Acta Volcanol 2:267–276

Koçaarslan A, Ersoy EY (2018) Petrologic evolution of Miocene–Pliocene mafic volcanism in the Kangal and Gürün basins (Sivas–Malatya), central east Anatolia: evidence for Miocene anorogenic magmas contaminated by continental crust. Lithos 310–311:392–408. https://doi.org/10.1016/j.lithos.2018.04.021

Koçyiğit A, Yılmaz A, Adamia S, Kuloshvili S (2001) Neotectonics of East Anatolian Plateau (Turkey) and Lesser Caucasus: implication from transition from thrusting to strike-slip faulting. Geodin Acta 14:177–195. https://doi.org/10.1016/S0985-3111(00)01064-0

Kürkçüoğlu B, Pickard M, Şen P, Hanan BB, Sayit K, Plummer C, Sen E, Yurur T, Furman T (2015) Geochemistry of mafic lavas from Sivas, Turkey and the evolution of Anatolian lithosphere. Lithos 232:229–241. https://doi.org/10.1016/j.lithos.2015.07.006

Kurt H, Asan K, Ruffet G (2008) The relationship between collision-related calcalkaline, and within-plate alkaline volcanism in the Karacadağ Area (Konya-Türkiye, Central Anatolia). Chem Erd Geochem 68:155–176. https://doi.org/10.1016/j.chemer.2006.05.003

Kürüm S, Önal A, Boztuğ D, Spell T, Arslan M (2008) ^{40}Ar/^{39}Ar age and geochemistry of the post-collisional Miocene Yamadağ volcanics in the Arapkir area (Malatya Province), eastern Anatolia, Turkey. J Asian Earth Sci 33:229–251. https://doi.org/10.1016/j.jseaes.2007.12.001

Le Maitre RW (2002) Igneous rocks. A classification and glossary of terms, 2nd edn. Cambridge University Press, Cambridge, p 236

Lee C-TA, Luffi P, Plank T, Dalton H, Leeman W (2009) Constraints on the depths and temperatures of basaltic magma generation on Earth and other terrestrial planets using new thermobarometers for mafic magmas. Earth Planet Sci Lett 279:20–33. https://doi.org/10.1016/j.epsl.2008.12.020

Lustrino M, Wilson M (2007) The circum-Mediterranean anorogenic Cenozoic igneous province. Earth Sci Rev 81:1–65. https://doi.org/10.1016/j.earscirev.2006.09.002

McNab F, Ball PW, Hoggard MJ, White NJ (2018) Neogene uplift and magmatism of anatolia: insights from drainage analysis and basaltic geochemistry. Geochem Geophys Geosyst 19:175–213. https://doi.org/10.1002/2017GC007251

Middlemost EAK (1975) The basalt clan. Earth Sci Rev 11:337–364. https://doi.org/10.1016/0012-8252(75)90039-2

Niu YI, O'Hara MJ (2008) Global correlations of ocean ridge basalt chemistry with axial depth: a new perspective. J Petrol 49:633–664. https://doi.org/10.1093/petrology/egm051

Notsu K, Fujitani T, Ui T, Matsuda J, Ercan T (1995) Geochemical features of collision-related volcanic rocks in central and eastern Anatolia, Turkey. J Volcanol Geotherm Res 64:171–192. https://doi.org/10.1016/0377-0273(94)00077-T

Okay AI (2008) Geology of Turkey: A synopsis. Anschnitt 21:19–42

Ottria G, Pandolfi L, Catanzariti R, Da Prato S, Ellero A, Frassi C, Göncüoğlu MC, Marroni M, Ruffini L, Sayit K (2017) Evolution of an early Eocene pull-apart basin in the Central Pontides (Northern Turkey): new insights into the origin of the North Anatolian Shear Zone. Terra Nova 29:392–400. https://doi.org/10.1111/ter.12299

Parlak O, Delaloye M, Demirkol C, Ünlügenç UC (2001) Geochemistry of Pliocene/Pleistocene basalts along the Central Anatolian Fault Zone (CAFZ), Turkey. Geodin Acta 14:159–167. https://doi.org/10.1016/S0985-3111(00)01062-7

Pearce TH (1978) Olivine fractionation equations for basaltic and ultrabasic liquids. Nature 276:771–774

Pearce JA (1982) Trace element characteristics of lavas from destructive plate boundaries. In: Thorpe RS (ed) Orogenic andesites and related rocks. Wiley, Oxford, pp 528–548

Pearce JA, Bender JF, DeLong SE, Kidd WSF, Low PJ, Güner Y, Saroğlu F, Yılmaz Y, Moorbath S, Mitchell JG (1990) Genesis of collision volcanism in Eastern Anatolia, Turkey. J Volcanol Geotherm Res 44:189–229. https://doi.org/10.1016/0377-0273(90)90018-B

Plank T, Forsyth DW (2016) Thermal structure and melting conditions in the mantle beneath the Basin and Range province from seismology and petrology. Geochem Geophys Geosyst 17:1312–1338. https://doi.org/10.1002/2015GC006205

Plank T, Langmuir CH (1998) The chemical composition of subducting sediment and its consequences for the crust and mantle. Chem Geol 145:325–394. https://doi.org/10.1016/S0009-2541(97)00150-2

Platzman ES, Tapirdamaz C, Sanver M (1998) Neogene anticlockwise rotation of central Anatolia (Turkey): preliminary palaeomagnetic and geochronological results. Tectonophysics 299:175–189. https://doi.org/10.1016/S0040-1951(98)00204-2

Poisson A, Vrielynck B, Wernli R, Negri A, Bassetti MA, Büyükmeriç Y, Özer S, Guillou H, Kavak KS, Temiz H, Orszag-Sperber F (2016) Miocene transgression in the central and eastern parts of the Sivas Basin (Central Anatolia, Turkey) and Cenozoic palaeogeographical evolution. Int J Earth Sci 105:339–368. https://doi.org/10.1007/s00531-015-1248-1

Reid M, Schleiffarth WK, Cosca MA, Delph JR, Blichert-Toft J, Cooper KM (2017) Shallow melting of MORB-like

mantle under hot continental lithosphere, Central Anatolia. Geochem Geophys Geosyst 18:1866–1888. https://doi.org/10.1002/2016GC006772

Reid MR, Delph JR, Cosca MA, Schleiffarth WK, Kuşku (2019) Melt equilibration depths as sensor of lithospheric thickness during Eurasia-Arabia collision and the uplift of the Anatolian Plateau. Geology 47:943–947. https://doi.org/10.1130/G46420.1

Salters VJM, Stracke A (2004) Composition of the depleted mantle. Geochem Geophys Geosyst 5:1–27. https://doi.org/10.1029/2003GC000597

Schildgen TF, Yıldırım C, Cosentino D, Strecker MR (2014) Linking slab break-off, Hellenic trench retreat, and uplift of the Central and Eastern Anatolian plateaus. Earth Sci Rev 128:147–168. https://doi.org/10.1016/j.earscirev.2013.11.006

Seghedi I, Maţenco L, Downes H, Mason PRD, Szakács A, Pécskay Z (2011) Tectonic significance of changes in post-subduction Pliocene-Quaternary magmatism in south east part of the Carpathian-Pannonian Region. Tectonophysics 502:146–157. https://doi.org/10.1016/j.tecto.2009.12.003

Şengör AMC, Gorür N (1985) Strike-slip faulting and related basin formation in zones of tectonic escape: Turkey as a case study. In: Biddle K, Christie-Blick N, (eds) Strike-slip deformation, basin formation and sedimentation, SEPM Sp Publ, Tulsa, vol 37, pp 227–264. https://doi.org/10.2110/pec.85.37.0211

Şengör AMC, Yılmaz Y (1981) Tethyan evolution of Turkey: a plate tectonic approach. Tectonophysics 75:181–241. https://doi.org/10.1016/0040-1951(81)90275-4

Şengör AMC, Özeren S, Genç T, Zor E (2003) East Anatolian high plateau as a mantle supported, north south shortened domal structure. Geophys Res Lett 30:8045. https://doi.org/10.1029/2003GL017858

Şengör AMC, Tüysüz O, İmren C, Sakinç M, Eyidoğan H, Görür N, Le Pichon X, Ranging C (2005) The North Anatolian Fault; a new look. An Rev Earth Planet Sci 33:37–112. https://doi.org/10.1146/annurev.earth.32.101802.120415

Shaw DM (1970) Trace element fractionation during anatexis. Geochim Cosmochim Acta 34:237–243. https://doi.org/10.1016/0016-7037(70)90009-8

Spera FJ, Bohrson WA (2001) Energy-constrained open system magmatic process I: general model and energy-constrained assimilation and fractional crystallization/EC-AFC) formulation. J Petrol 42:999–1018. https://doi.org/10.1093/petrology/42.5.999

Stormer JC, Nicholls J (1978) XLFRAC: a program for the interactive testing of magmatic differentiation models. Comput Geosci 4:143–159. https://doi.org/10.1016/0098-3004(78)90083-3

Sun SS, McDonough WF (1989) Chemical and isotopic systematics of oceanic basalts: implications for mantle composition and processes. Geol Soc Spec Publ 42:313–345. https://doi.org/10.1144/GSL.SP.1989.042.01.19

Tatar O, Yurtmen S, Temiz H, Gürsoy H, Koçbulut F, Mesci BL, Guezou JC (2007) Intracontinental Quaternary volcanism in the Niksar pull-apart basin, North Anatolian fault zone, Turkey. Turk J Earth Sci 16:417–440

Tatsumi Y, Hamilton DL, Nesbitt RW (1986) Chemical characteristics of fluid phase released from a subducted lithosphere and origin of arc magmas: evidence from high-pressure experiments and natural rocks. J Volcanol Geotherm Res 29:293–309. https://doi.org/10.1016/0377-0273(86)90049-1

Taylor SR, McLennan SM (1985) The continental crust: its composition and evolution. Blackwell, Oxford, p 312

Thirlwall MF, Upton BGJ, Jenkins C (1994) Interaction between Continental Lithosphere and the Iceland Plume—Sr–Nd–Pb Isotope Geochemistry of Tertiary Basalts, NE Greenland. J Petrol 35:839–879. https://doi.org/10.1093/petrology/35.3.839

Toprak V (1994) Central Kızılırmak Fault Zone: northern margin of Central Anatolian Volcanics. Turk J Earth Sci 3:29–38

Toscani L, Salvioli-Mariani E, Mattioli M, Tellini C, Boschetti T, Iacumin P, Selmo E (2020) The pyroclastic breccia of the Cabezo Negro de Tallante (SE Spain): the first finding of carbonatite volcanism in the Internal Domain of the Betic Cordillera. Lithos 354:105288. https://doi.org/10.1016/j.lithos.2019.105288

Uluocak EŞ, Pysklywec R, Göğüş OH (2016) Present-day dynamic and residual topography in Central Anatolia. Geophys J Int 206:1515–1525. https://doi.org/10.1093/gji/ggw225

Varol E, Temel A, Yürür T, Gourgaud A, Bellon H (2014) Petrogenesis of the Neogene bimodal magmatism of the Galatean Volcanic Province, Central Anatolia, Turkey. J Volcanol Geotherm Res 280:14–29. https://doi.org/10.1016/j.jvolgeores.2014.04.014

Westaway R (2003) Kinematics of the Middle East and Eastern Mediterranean Updated. Turk J Earth Sci 12:5–46

Westaway R, Arger J (2001) Kinematics of the Malatya-Ovacik Fault Zone. Geodin Acta 14:103–131. https://doi.org/10.1016/S0985-3111(00)01058-5

White R, McKenzie D (1989) Magmatism at rift zones: the generation of volcanic continental margins and flood basalts. J Geophys Res Solid Earth 94(B6):7685–7729. https://doi.org/10.1029/JB094iB06p07685

Wilson M, Tankut A, Guleç N (1997) Tertiary volcanism of the Galatia province, north-west Central Anatolia, Turkey. Lithos 42:105–121. https://doi.org/10.1016/S0024-4937(97)00039-X

Workman RK, Hart SR (2005) Major and trace element composition of the depleted MORB mantle (DMM). Earth Planet Sci Lett 231:53–72. https://doi.org/10.1016/j.epsl.2004.12.005

Yağmurlu F, Toker E, Şentürk M (2016) The coal-quality distribution of lignite deposits and tectono-sedimentary evolution of Etyemez in Kangal Neogene basin (Central Anatolia, Turkey). Int J Oil Gas Coal T 11:75–92. https://doi.org/10.1504/IJOGCT.2016.073781

Yalçin H, Gündoğdu MN, Gourgaud A, Vidal P, Uçurum A (1998) Geochemical characteristics of Yamadağı volcanics in central east Anatolia: an example from collision-zone volcanism. J Volcanol Geotherm Res 85:303–326. https://doi.org/10.1016/S0377-0273(98)00061-4

Yılmaz A (1994) An example of a post-collisional trough: Sivan Basin, Turkey. In: Proceedings of the 10th petroleum congress of Turkey. Turkish Ass Petrol Geol Publ, pp 21–32

Yılmaz Y, Polat A (1998) Geology and evolution of the Thrace volcanism, Turkey. Acta Vulcanol 10:293–303

Yılmaz Y, Güner Y, Şaroğlu F (1998) Geology of the quaternary volcanic centres of the east Anatolia. J Volcanol Geotherm Res 85:173–210. https://doi.org/10.1016/S0377-0273(98)00055-9

Zindler A, Hart S (1986) Chemical Geodynamics. Ann Rev Earth Planet Sci 14:493–571. https://doi.org/10.1146/annurev.ea.14.050186.002425

Authors and Affiliations

Paolo Di Giuseppe[1] · Samuele Agostini[1] · Gianfranco Di Vincenzo[1] · Piero Manetti[2] · Mehmet Yilmaz Savaşçın[3] · Sandro Conticelli[2,4,5]

[1] CNR, Istituto di Geoscienze e Georisorse, Via Moruzzi, 1, 56124 Pisa, Italy

[2] Dipartimento di Scienze della Terra, Università degli Studi di Firenze, Via Giorgio La Pira, 4, 50121 Florence, Italy

[3] Jeoloji Mühendisliği Bolümü, Munzur Üniversitesi, 62000 Tunceli, Turkey

[4] CNR, Istituto di Geoscienze e Georisorse, Sede Secondaria di Firenze, Via Giorgio La Pira, 4, 50121 Florence, Italy

[5] CNR, Istituto di Geologia Ambientale e Geoingegneria, Area Della Ricerca di Roma1-Montelibretti, Via Salaria Km 29,300, 00015 Monterotondo, RM, Italy